

# Continental-scale prediction of hydrologic signatures and processes

Ryoko Araki<sup>1,2</sup>, Anne Holt<sup>1</sup>, John C. Hammond<sup>3</sup>, Admin Husic<sup>4</sup>, Gemma Coxon<sup>5</sup>, Hilary K. McMillan<sup>1</sup>

<sup>1</sup>Department of Geography, San Diego State University, San Diego, CA, USA.

<sup>2</sup>Department of Geography, University of California, Santa Barbara, Santa Barbara, CA, USA.

<sup>3</sup>U.S. Geological Survey, Maryland–Delaware–DC Water Science Center, Baltimore, MD, USA.

<sup>4</sup>Department of Civil and Environmental Engineering, Virginia Tech, Blacksburg, VA, USA.

<sup>5</sup>School of Geographical Sciences, University of Bristol, Bristol, UK.

*Correspondence to:* Ryoko Araki (raraki8159@sdsu.edu; raraki@ucsb.edu) and Hilary McMillan (hmcmillan@sdsu.edu)

**Abstract.** Understanding how dominant hydrologic processes and their drivers vary across diverse continental-scale landscapes is critical for hydrologic modeling and water management applications. Our research addresses this question by synthesizing large-sample watershed datasets, Caravan and GAGES-II, and developing random forest models to identify patterns in hydrologic function. We assessed dominant processes by examining hydrologic signatures—summary indicators of watershed function derived from hydroclimatic time series and random forest models across 14,146 gauged [United States](#) watersheds. The results reveal clear continental-scale gradients in hydrologic processes, including baseflow, overland flow, storage, and water balance losses. Our map of dominant processes highlights, for example, the transition from baseflow to fast responses and back to baseflow along the elevation gradient from the Appalachian spine, through the Piedmont, to the Eastern Coastal Plain; a distinct outer ring around the Great Lakes region; and sharp contrasts between coastal and inland processes in the West. Variable importance analysis from random forest models show that processes in the western U.S. are primarily controlled by climate, whereas in the eastern U.S., soil, geology, and topography play larger roles, with distinct human influences apparent in urban areas. Our approach of estimating dominant processes and their drivers facilitates extending process knowledge from research watersheds to the continental scale, assessing current hydrological understanding, and evaluating hydrological model structures.

## 1 Introduction

### 1.1 Identifying hydrologic processes at large scales

Estimating the contributions of different hydrologic processes to streamflow generation at a continental scale is essential for flood forecasting and water resources management. Optimal management strategies, including the design of grey and green infrastructure, differ depending on which processes dominate hydrological response (Oswald et al., 2023; Thompson et al., 2020), which vary substantially by regional environmental conditions (Blöschl, 2006; Paola et al., 2006; Penna, 2024). Understanding how water is partitioned, stored, and transported through different parts of the terrestrial systems is a fundamental question in the hydrologic sciences (Brooks et al., 2015). To simulate a diverse set of processes at large-scale, a new generation of hydrologic models with flexible and heterogeneous structures has emerged (Clark et al., 2015; Frame et al., 2025; Johnson et al., 2023). However, despite these technological advances, we still lack an estimate of dominant hydrologic

34 processes controlling streamflow generation at continental scales (McMillan et al., 2025; Reinecke et al., 2025). Developing  
35 this understanding is a critical step toward unified hydrologic theory (Sivapalan, 2005) and can provide a blueprint for robust  
36 model development and informed decision making.

37  
38 Previous efforts to map multiple hydrologic processes at continental scales are scarce. Most large-scale studies have focused  
39 on one process. For example, Buchanan et al., (2018) assessed the likelihood of infiltration excess flow occurrence by  
40 comparing whether rainfall intensity exceeds saturated hydraulic conductivity, finding that saturation excess dominates across  
41 the contiguous [United States \(U.S.\)](#), while infiltration excess is regionally likely in the central U.S. Similarly, studies on  
42 baseflow indices have shown their strong dependence on climatic and soil properties (Beck et al., 2013; Xie et al., 2024), and  
43 Fang and Shen (2017) quantified the runoff-storage connectivity through correlations between anomalies in streamflow gauge  
44 and satellite water storage observations, highlighting large-scale interactions among groundwater table, soil thickness,  
45 topography, and snow. In contrast, studies that examined multiple processes have been typically focused on a single or small  
46 groups of watersheds. A study in Alaska shows that the use of multiple streamflow statistics can help distinguish and assign  
47 hydrologic regions (Barnhart et al., 2022). [One of the few studies to holistically investigate storm runoff generation at  
48 continental scales \(Wu et al., 2021\) demonstrates that large-sample analysis aligns with previous conceptual understanding of  
49 runoff mechanisms across landscapes \(Dunne et al., 1978\) while highlighting the roles of precipitation volume and geology.](#)  
50 Model-aided studies have simulated global patterns of multiple indices: water partitioning into green and blue water,  
51 streamflow response elasticity to rainfall, and streamflow flashiness (Ji et al., 2025), U.S.-wide indices for water balance  
52 seasonality (Berghuijs et al., 2014). Another model-based approach has involved inferring hydrologic processes through  
53 parameter sensitivity analysis (Hay et al., 2023). These synthesis studies present promising descriptions of spatial patterns and  
54 directions for future progress toward a holistic understanding of runoff generation mechanisms, which still remains elusive.

55  
56 Much of the research for generalizing watershed function has focused on summarizing flow regimes (Dettinger and Diaz,  
57 2000; Lane et al., 2017; Lee et al., 2015; Lins, 1997) and predicting shifts in flow regime under future climate (Brunner et al.,  
58 2020; Hodgkins et al., 2024). Many studies cluster streamflow gauges using flow indices that target general (Almagro et al.,  
59 2024; Ariano and Ali, 2025; Mosley, 1981; Wu et al., 2021), intermittent (Sauquet et al., 2021), or seasonal streamflow patterns  
60 (Dhungel et al., 2016; Haines et al., 1988; Kennard et al., 2010). However, most of these studies aim to define the similarity  
61 of flow regimes rather than the underlying runoff generation processes. Furthermore, the results from clustering approaches  
62 are constrained to gauged locations and lack spatial coherence, making it challenging to extrapolate to ungauged watersheds.

63  
64 To estimate watershed processes in ungauged locations, hydrologists have conventionally used maps derived from  
65 physiographic datasets. For example, in the United States context, the Environmental Protection Agency's Ecoregions  
66 (Omernik, 1987, 2004), an ecosystem classification based on the physical and biotic characteristics, is a common reference  
67 when discussing hydrologic processes (Falcone et al., 2010). Other classifications include the United States Geological

68 Survey's Water Resources Regions (Seaber et al., 1987) based on streamflow networks, Hydrologic Landscape Regions  
69 (Santhi et al., 2008; Winter, 2001; Wolock, 2003a) based on physiographic and climatic datasets, and the United States  
70 Department of Agriculture's Hydrologic Soil Groups (Web Soil Survey, 2025) based on soil surveys. Nevertheless,  
71 regionalization based on physiographic data often fails to capture the full variability of watershed function (Ali et al., 2012;  
72 Oudin et al., 2008) because hydrologic processes can differ even among physiographically similar watersheds (McMillan et  
73 al., 2014). Capturing watershed processes at a continental scale calls for a scalable method to draw information from  
74 hydroclimatic datasets. To date, no studies have attempted to develop comprehensive maps of runoff generation processes  
75 based on streamflow observations that can effectively capture watersheds' functions.

#### 76 **1.2 Hydrologic signatures links to processes**

77 Hydrologic signatures are metrics that quantify hydrologically-relevant dynamics, and offer a promising way to infer watershed  
78 processes with minimal data requirements (McMillan, 2021). Hydrologic signature calculations require only widely-available  
79 datasets, such as streamflow and precipitation, and can be related to various watershed processes, such as runoff generation  
80 and water storage dynamics (McMillan, 2020; Wlostowski et al., 2021). Using hydrologic signatures, expert knowledge, and  
81 landscape characteristics, Fenicia and McDonnell (2022) inferred dominant runoff processes and developed perceptual models  
82 at the regional scale; and Pechlivanidis and Arheimer (2015) mapped process differences at the national scale in India.  
83 Hydrologic signatures can capture the functional streamflow responses to climatic forcings and can discriminate different  
84 processes across landscapes (Araki et al., 2022; Gnann et al., 2020, 2021a; Janssen and Ameli, 2021). This enables a signature-  
85 based exploration of the relationship between landscape form and function (Bracken et al., 2013; Sivapalan, 2005).

#### 86 **1.3 Predicting hydrologic signatures using watershed attributes**

87 Watershed attributes describe the physical characteristics of watersheds, which can be used to identify the drivers of hydrologic  
88 processes and to transfer hydrological knowledge to ungauged locations (Tarasova et al., 2023). The link between watershed  
89 attributes and signatures of streamflow response can be explored via machine learning approaches on large watershed samples.  
90 Regional and global applications include studies in the U.S. (Addor et al., 2018; Janssen and Ameli, 2021; Wu et al., 2021),  
91 Australia (Trancoso et al., 2017), Zimbabwe (Mazvimavi et al., 2005), Brazil (Almagro et al., 2024), Europe (Rudlang et al.,  
92 2025; Kuentz et al., 2017), and globally (Beck et al., 2015). Across all studies, climate emerged as the primary control on  
93 signatures. Non-climatic factors (i.e., landscape attributes), such as soil, geology, vegetation cover, and topography, had weak  
94 or limited predictive power. However, substantial evidence from field-based studies shows that landscape forms are a primary  
95 control of watershed function (Angermann et al., 2017; Fan et al., 2019; Jackisch et al., 2017; Jefferson et al., 2010; Lohse and  
96 Dietrich, 2005; Pfister et al., 2017; Zimmer and Gannon, 2018).

97  
98 Weak predictive power of non-climatic drivers can be attributed to lack of high-resolution, accurate landscape attributes that  
99 describe regionally important processes (Gnann et al., 2021a; Tarasova et al., 2023). For example, wetlands are key regulators

of low flows in the U.S. (Worland et al., 2018) and have been left out of previous studies (Addor et al., 2018). Similarly, weathering and glaciation have primary impacts on baseflow storage and generation (Neff et al., 2005; Tague and Grant, 2004), but rock permeability and porosity predictors did not clearly capture the relationship (Wu et al., 2021). Coarse spatial resolution, or limited quality and consistency of global datasets may reduce their predictive power (Nascimento et al., 2025; Beck et al., 2015). Additionally, large-sample studies across broad climatic gradients may be obscuring the influences of landscape attributes. Regional analysis can mitigate this effect and elucidate the non-climatic drivers; for example, regional random forest models have revealed physiographic and anthropogenic controls on flow regimes (Almagro et al., 2024; Hammond et al., 2021). However, smaller regional sample sizes may limit prediction accuracy if datasets only provide tens of watersheds per region (Willard et al., 2024).

Lastly, the quality of signatures can compromise data-driven model performance and interpretation for process understanding. Examples include the sensitivity of flow duration curve slope to measurement errors (McMillan et al., 2017), the sensitivity of signatures to rating curve uncertainties (Westerberg et al., 2016), lack of process representativeness (McMillan et al., 2022), and inaccurate parameterization of storm separation algorithms (McMillan et al., 2023). Minimizing the impact of signature uncertainty is important for differentiating different regional watershed functionalities (Westerberg et al., 2016).

#### 1.4 Aims of the paper

This study presents the first hydrologic processes map for the contiguous United States (CONUS). We synthesized hydrologic signatures as process indicators, going beyond pattern identification from single signatures. We hypothesize that signature combinations can represent six key hydrologic processes (McMillan, 2020; McMillan et al., 2022): baseflow and storage, water balance and seasonal flow variability, and saturation and infiltration excess overland flow. Using random forest models, we demonstrate the explanatory power of landscape metrics to predict hydrologic signatures and their regional variations, and thus the underlying processes, across CONUS.

We address the limitations of previous studies in predicting hydrologic signatures. First, we improved the quality of non-climatic attributes by: (i) incorporating new geological and wetland landscape attributes that have demonstrated strong connections to baseflow processes (Holt and McMillan, 2025); and (ii) utilizing watershed attributes from GAGES-II datasets (Falcone, 2011), derived from survey-based and higher-resolution products. Second, we interpret random forests using Shapley values (Shapley, 1953) following Husic et al. (2025), as well as permutation importance values within a regional model-building approach, following Hammond et al. (2021), which extends prior work to elucidate the regional contributions of non-climatic, landscape attributes to hydrologic processes. Furthermore, our work assessed 14,146 U.S. watersheds and was trained on 10,261 watersheds, nearly ten times more sample watersheds than previous studies; we leverage the Caravan and GAGES-II—the most extensive open-source large-sample datasets currently available (Falcone, 2011; Kratzert et al., 2023). Third, we utilize a set of hydrologic signatures proven robust across large-sample watershed studies and have a clear connection to

133 critical-zone processes (McMillan et al., 2022), with their parameters further tuned to local storm characteristics. With these  
134 improvements, we expand watershed coverage and uncover more detailed spatial patterns of watershed processes than  
135 previously possible, using widely-available hydroclimatic datasets and physiographic attributes.

## 136 **2 Data**

137 We used two primary sources of streamgages and watershed attribute data to expand the number of samples: Caravan v1.5  
138 (Kratzert et al., 2023, 2024) and U.S. Geological Survey GAGES-II (Falcone, 2011; Falcone et al., 2010). See Fig. 1 for the  
139 spatial distribution of the study watersheds. Caravan is an open-source dataset of global watersheds; its CONUS subset consists  
140 of 9,234 watersheds sourced from CAMELS-US (Addor et al., 2017) and HYSETS (Arsenault et al., 2020). GAGES-II is a  
141 geospatial dataset of 9,067 watersheds in the United States, selected for their quality to characterize natural and altered flow  
142 regimes.

### 143 **2.1 Hydroclimatic dataset**

144 We calculated hydrologic signatures listed in Table 1 using daily hydroclimatic timeseries data from watersheds within the  
145 contiguous United States (CONUS). For Caravan watersheds, we used U.S. Geological Survey (USGS) streamflow  
146 measurements paired with daily ERA5-Land forcings provided. For the GAGES-II watersheds, we obtained the USGS  
147 streamflow records (U.S. Geological Survey, 2025) using the dataRetrieval package (DeCicco et al., 2018) and gridMET  
148 forcings from Wiczorek et al. (2023). For calculating infiltration excess overland flow signatures of Wu et al. (2021);  
149 “*RC\_Pint*”), we used the hourly precipitation from the North American Land Data Assimilation System 2 (NLDAS-2; Xia et  
150 al., 2012) provided through CAMELSH: a Large-Sample Hourly Hydrometeorological Dataset and Attributes at Watershed-  
151 Scale for CONUS (Tran, 2025; Tran et al., 2025).

### 152 **2.2 Watershed attributes**

153 We combined watershed attributes from three sources: (1) Caravan, (2) GAGES-II, and (3) geologic age and wetland attributes  
154 (Holt and McMillan, 2025). We added average geologic age and isolated wetland fraction metrics because of their strong link  
155 to baseflow processes, which were missing from previous large-sample analyses (Holt and McMillan, 2025). From the Caravan  
156 and Holt & McMillan (2025) attribute sets, we excluded binary or categorical attributes, monthly climate variables,  
157 uninformative attributes for the CONUS context (e.g., permafrost extent, gross domestic product), and highly correlated  
158 attributes (Spearman's  $\rho > 0.8$  or  $< -0.8$ ; see Text S1). Where available, Caravan attributes were substituted with GAGES-II  
159 attributes, as described in Section 3.2 and Table S1. Table 2 lists the 23 attributes used in the random forest analysis. The  
160 purpose of merging Caravan and GAGES-II dataset is to maximize the sample size of watersheds and better capture regional  
161 hydrologic variability (see Table S1 and an associated Venn diagram of watershed coverage across datasets).

162 **3 Method**

163 We analyzed 14,146 gauged U.S. watersheds; our map of processes was based on observational data from 10,261 gauged sites  
164 and extended using random forest predictions to an additional 3,885 watersheds. See Table S1 and associated figures for an  
165 overview of the datasets used and the workflow.

166 **3.1 Calculating hydrologic signatures**

167 A total of 12 signatures (four baseflow and groundwater signatures, four water balance and seasonality-related signatures, and  
168 four overland flow signatures) were used to characterize hydrologic dynamics (see Table 1). The signatures were selected  
169 based on their reliability in representing processes (McMillan et al., 2022). We calculated signatures using the TOSSH toolbox  
170 (Gnann et al., 2021b) and tuned the parameters for event separation for each hydroclimatic region (see Tables S2, S3).

171  
172 We filtered out watersheds from our signature calculations based on quality criteria for watershed area and snow used by  
173 previous studies, and on the timeseries length needed for signatures to stabilize. First, we removed watersheds from our analysis  
174 with uncertain topographic boundaries, showing high discrepancies (>25%) in the estimated drainage area between GAGES-  
175 II and Caravan datasets. Errors of <20% are possible due to differences in watershed delineation tools or missing small  
176 tributaries (Ray, 2018). Second, for overland flow signature analysis, we excluded snow-dominated watersheds (>20% snow  
177 fraction of total precipitation; a >30% criterion were used in McMillan et al., 2022 and Wu et al., 2021); this is because our  
178 overland flow signatures can be heavily influenced by periods with no flow response due to snow or frozen conditions. Third,  
179 we excluded watersheds with less than 5 years of streamflow observation record, and those with over 30% missing daily data  
180 over the period where streamflow was recorded (yielding at least three years of available data). Studies suggest that temporal  
181 hydrologic variability is adequately captured with 3 to 5 years of data (Refsgaard and Storm, 1996; Klemeš, 1986; Merz et al.,  
182 2009).

183 **3.2 Training random forest models and predicting hydrologic signatures**

184 We developed random forest models to examine potential drivers of hydrologic processes. Random forest models have been  
185 widely used for this task (Eng and Wolock, 2022; Lapidés et al., 2023; Zipper et al., 2021) for their interpretability, relatively  
186 low computational demands, and robustness to multi-collinearity (Addor et al., 2018). For each signature, we constructed a  
187 random forest model to predict its values based on watershed attributes using the caret R package (Kuhn, 2008; R Core Team,  
188 2024). Each model used 500 trees with the optimal number of features randomly resampled at each split, selected by  
189 minimizing root mean squared error (RMSE) through 10-fold cross-validation.

190  
191 Only the signatures calculated from quality-controlled streamflow records (as described in Section 3.1) were used for training.  
192 Training on all Caravan watersheds yielded  $R^2 < 0.4$  for many of the signatures, so we limited the training samples to the 4,748

Formatted: Normal

193 Caravan watersheds with streamflow gauge IDs overlapping with GAGES-II to attain model performance comparable to  
194 previous studies (see Text S2). When a gauged watershed was present in both datasets, we prioritized CAMELS over HYSETS,  
195 and Caravan over GAGES-II. This is to ensure the broader applicability of our method across different countries, as Caravan  
196 is available at global scale. This yielded a total 14,146 watersheds for signature analysis (overview in Table S1).

197  
198 We then used the trained model to predict hydrologic signatures for 3,885 watersheds where observations did not meet data  
199 quality standards as described in Section 3.1. Previous study (do Nascimento et al., 2025) and our preliminary experiments  
200 (Text S2) showed improved model performance when the watershed attributes were derived from higher-resolution datasets  
201 based on detailed field surveys, such as in GAGES-II and Holt and McMillan, (2025). Therefore, we used GAGES-II attributes  
202 and when unavailable, used the coarser resolution Caravan attributes (see Table S1).

### 203 **3.3 Interpretation of hydrologic signatures as process descriptors**

204 We combined signatures calculated from observed streamflow data and predicted with random forest models to develop a  
205 comprehensive map of processes for watersheds across the U.S. (Fig. 1). A bivariate space of hydrologic signatures was used  
206 to infer process dominance. For each selected process, we used the two signatures most strongly related to the process inferred  
207 from previous work (Bolotin and McMillan, 2024; McMillan, 2020; McMillan et al., 2022; Wu et al., 2021). Each signature  
208 was categorized based on the quantiles of signatures, from low (0-25%), mid-low (25-50%), mid-high (50-75%), to high (75-  
209 100%). When both of the two target signatures had mid-high (50-75%) or high (75-100%) values, we interpreted this as  
210 indicative of process dominance. This bivariate matrix can highlight the complexity of hydrologic processes where two  
211 signatures do not necessarily show the same trends.

212  
213 The process hypotheses tested are described in Table 1 and cover six major hydrologic processes: baseflow, watershed storage,  
214 water balance, seasonal variability, overland flow dominance, and its type. Baseflow sustains discharge across seasons and  
215 reflects groundwater connectivity, while overland flow drives stormflow and influences flood peaks. Storage governs buffering  
216 and recession dynamics, and water balance losses through evapotranspiration and deep percolation determine how much  
217 precipitation is converted to streamflow. Together, these processes span the continuum from slow to fast hydrologic response  
218 and integrate both vertical and lateral fluxes, making them essential for hydrologic theory and modelling (Bergström, 1992;  
219 Kirchner et al., 2009; Berghuijs et al., 2014).

### 220 **3.4 Interpretation of process drivers using Shapley values**

221 We quantified feature importance using Shapley values (Shapley, 1953), which provide a robust and consistent measure to  
222 interpret random forest models (Lundberg et al., 2018). Shapley values represent the average marginal contribution of a feature  
223 (i.e., a landscape attribute) to a prediction, given the effects from all combinations of the considered features. Shapley values  
224 allow for local and global interpretation of machine learning model predictions, helping to uncover site-specific and

225 generalizable linkages between hydrology and landscape features (Husic et al., 2025). We used the interpretable machine  
226 learning (iml) R package (Molnar et al., 2018) to calculate Shapley values over the training data.

227  
228 To evaluate the regional effects of watershed attributes, we computed summary statistics on Shapley values. Shapley values  
229 are site-specific:  $\phi_x^{(y,i)}$  is the Shapley value calculated for an attribute  $x$  for a signature  $y$  at location  $i$ . Summing the Shapley  
230 values across watershed attributes  $x$  at a single location gives the deviation of the predicted signature value  $y_i$  at location  $i$  from  
231 the mean signature value across all sites. To compare effects of a landscape attribute  $x$  across sites, we normalize Shapley  
232 values by the total absolute contribution from all attributes at a site  $i$ ; this gives a metric for the relative contribution of an  
233 attribute  $x$  to signature  $y$  at site  $i$  as:

$$R_x^{(y,i)} = |\phi_x^{(y,i)}| / \sum_{x \in A} |\phi_x^{(y,i)}|$$

234  
235 where  $A$  is the set of all watershed attributes, and  $|\cdot|$  denotes the absolute value. To investigate which types of landscape  
236 characteristics are influential, we classified the watershed attributes into five categories (see Table 2), namely, topography,  
237 land-cover, soil & geology, human alteration, and climate.

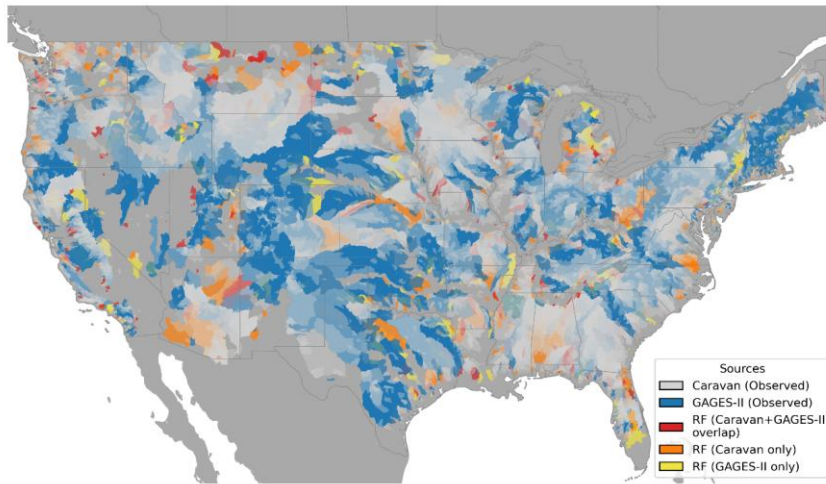
238  
239 Then, the average relative contribution of category  $k$  for signature  $y$  at location  $i$ ,  $\bar{R}_k^{(y,i)}$ , is calculated as:

$$\bar{R}_k^{(y,i)} = \frac{1}{K} \sum_{x \in C_k} R_x^{(y,i)}$$

240  
241 , where  $C_k$  is the set of watershed attributes belonging to category  $k$ , and  $K$  is the number of categories (in our case, five).

### 242 3.5 Interpretation of process drivers using permutation importance

243 To further evaluate locally important watershed attributes, we computed permutation importance, which measures the change  
244 in model performance when a feature (i.e., a landscape attribute) is removed. Prior work has shown that permutation  
245 importance derived from random forest models trained on regional samples is more effective than a continental approach for  
246 identifying physiographic, landscape controls on hydrologic responses, as it allows assessment under consistent climate  
247 conditions (Almagro et al., 2024; Hammond et al., 2021; Holt and McMillan, 2025). Therefore, we calculated permutation  
248 importance as the average changes in mean squared error (MSE), normalized by its standard deviation using the caret R  
249 package (Kuhn, 2008), from random forest models trained on regional watershed samples. Six climate regions were defined  
250 using a Gaussian mixture model in Scikit-learn (Pedregosa et al., 2011) based on relevant Caravan, GAGES-II, and Hammond  
251 et al. (2023) climate attributes (Table S4), and separate random forest models were trained for each region. Fig. S1 shows the  
252 identified climate regions.



254

255 **Figure 1: Method used to obtain hydrologic signatures. Signatures are derived either from observed data (“Observed”: Caravan**  
 256 **samples, n=7,465; GAGES-II samples, n=2,807; total n=10,261) or predicted using random forest models (“RF”; n=3,885). Predicted**  
 257 **samples are categorized as: “Caravan+GAGES-II overlap” (present in both the Caravan and GAGES-II datasets; n=618), “Caravan**  
 258 **only” (exclusive to Caravan; n=2,424), and “GAGES-II only” (exclusive to GAGES-II; n=843). State boundaries are indicated by**  
 259 **grey lines.**

260

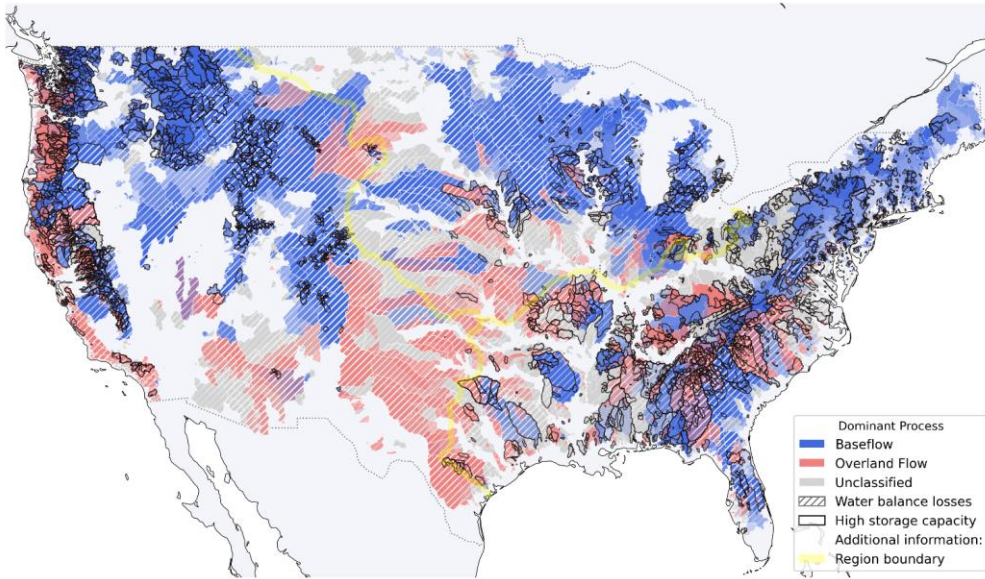
## 4 Results

261

### 4.1 Mapping dominant processes across the contiguous U.S.

262

263 Figures 2 and 3 show the maps of dominant processes derived from the hypotheses outlined in Table 1. Figure 2 presents the  
 264 signature of each process hypothesis in a bivariate map. Figure 3 provides a summary, displaying the four primary hydrologic  
 265 processes when it is deemed dominant (i.e. both signatures are in the mid-high (50-75 %) or high (75-100 %) quantiles).  
 266 Together, these maps highlight distinct regional patterns in hydrologic processes across the study area. The following sections  
 267 examine these patterns in greater detail by region: the East and South. (Section 4.2.1.), the Midwest and Central (Section 4.2.2.),  
 and the West and Southwest (Section 4.2.3.).



268

269

270

271

272

**Figure 2:** Map of dominant processes estimated based on our hypothesis (defined in Table 1 and Section 3.3). Note that when baseflow and overland flow both occur, their colors are overlaid to give purple hues. “Unclassified” means a watershed is deemed neither baseflow- nor overland-low-dominant. “Region boundary” indicates the areas described in Section 4.2.1-4.2.3 (East and South (bottom right), Midwest and Central, West and Southwest (left in the figure)).

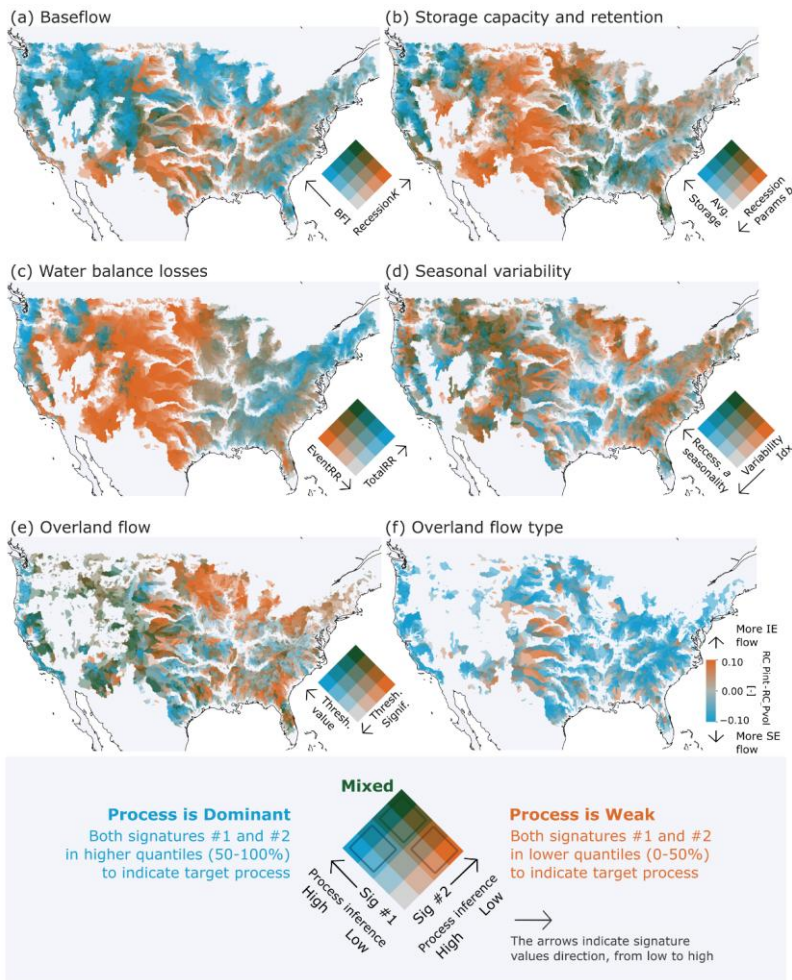


Figure 3: Hydrologic signatures of each process hypothesis, shown in bivariate maps (a-e). See the legend at the bottom for explanation. The high-process quantile from (a) is used to infer “Baseflow” in Figure 2; from (b) to infer

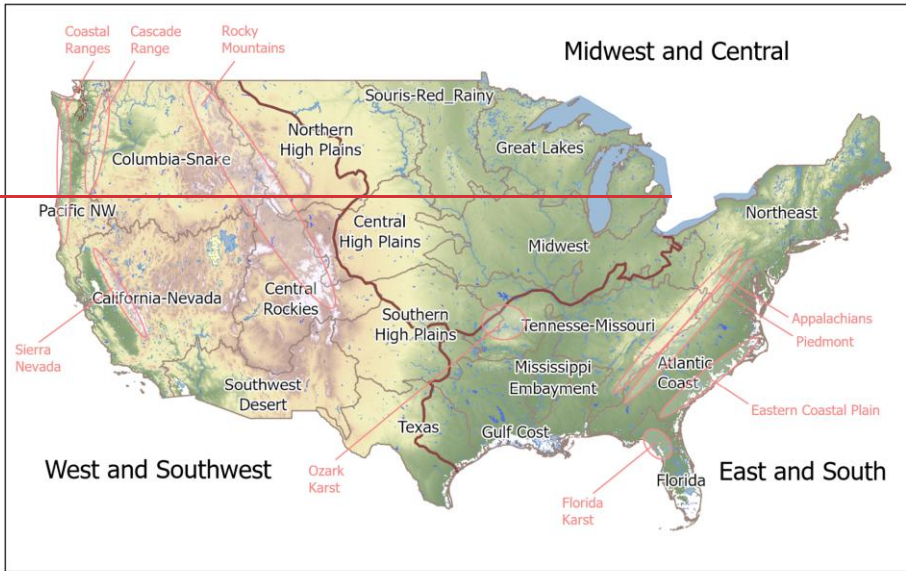
“High storage capacity”; from (c) to infer “Water balance losses”; and from (e) to infer “Overland flow.” Panel (f) shows the differences between the two signatures related to infiltration-excess (IE) flow and saturation-excess (SE) flow (i.e., values of  $IE$  Correlation ( $RC\_Pint$ ) minus  $SE$  Correlation ( $PC\_Pvol$ )). In the overland flow panels (e) and (f), watersheds dominated by snow (i.e.,

Formatted: Font: Italic

Formatted: Font: Not Italic

Formatted: Font: Italic

280 where more than 20% of annual total precipitation falls as snow) are not shown. For the overland flow type pane (f), watersheds are  
281 not shown when the correlations between the event runoff coefficient and both rainfall characteristics (i.e., storm rainfall volume  
282 and maximum intensity) are negative. For maps of each signature value, see Figures S2 and S3. [See Table 1 for signature names](#)  
283 [abbreviations](#).



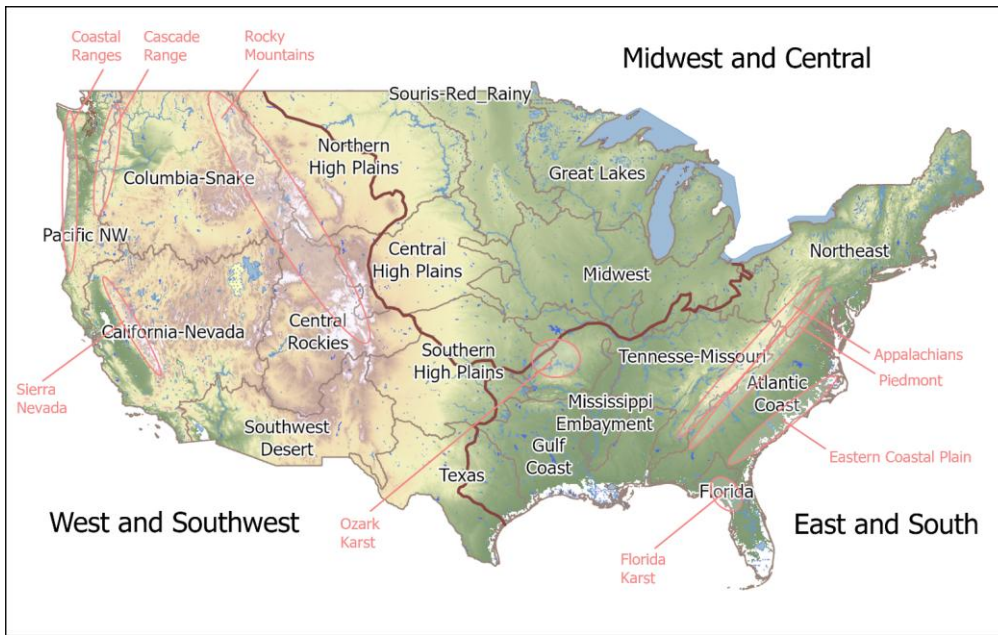


Figure 4: Map of the contiguous United States showing (i) areas described in Section 4.2.1-4.2.3 (East and South, Midwest and Central, West and Southwest; bolded brown line) (ii) geographical boundaries used for the USGS National Water Availability Assessment (Qi and Mason, 2023; Stets et al., 2025; Van Metre et al., 2020) (beige line) (iii) topographic and geological features named in the text (pink annotations).

## 4.2 Spatial patterns of hydrologic processes inferred from signatures

### 4.2.1 Region 1: East and South

This humid region has moderate to high precipitation (1,000-1,500 mm/yr; calculated based on the 10th and 90th percentiles of sample watershed attributes), with low precipitation seasonality except in Florida. Temperatures vary widely from snow-dominated areas in the NorthEast to subtropical areas in Florida, with mean annual temperature ranging from 7-19°C (Fig. S4). The landscape is old with deeply weathered soils and characterized by predominantly low-lying elevation (mean watershed elevation ranges between 40-600m), though there is a primary elevation gradient from the Appalachian Mountains and Piedmont to the Eastern coastal plains, with peaks exceeding 1,000m (Fig. S8). In Figure 3, signature values show that these climate and landscape conditions produce slowly-varying, baseflow-dominated flow regimes and mid-quantile signature values showing a lack of hydrologic extremes. Runoff ratios (*Total Runoff Ratio* and *Event Runoff Ratio*; Fig. 3c) are moderate or high and seasonal variability in flow and recessions is moderate to low. Storage capacity (*Average Storage*) is overall

301 moderate, but recession shapes (*Recession Parameters b*) are variable (Fig. 3b). Evidence for overland flow is weak with  
302 saturation excess prevailing when it occurs (Fig. 3e,f).

303  
304 The gradient along the geographical transect from the Appalachian spine to the Eastern coastal plain is apparent in several  
305 processes. The Appalachians have strong baseflow influence, shown by high baseflow index and slow recessions (Fig. 3a).  
306 Nonlinear recessions (high *Recession Parameter b*; Fig. 3b) indicate multiple groundwater reservoirs supplying baseflow. In  
307 contrast, the Piedmont has lower baseflows and fast recessions, relating to lower storage-. The Eastern coastal plain, especially  
308 towards the South, has high baseflow and moderate to slow recessions (Fig. 3a). Linear recessions suggest a single dominant  
309 groundwater reservoir supplying baseflow in this sandy, coastal plain aquifer (Fig. 3b). Lower runoff ratios in the coastal plains  
310 indicate losses to deep groundwater including offshore discharge, especially in Florida's karst area (Fig. 3c, S6). The karst  
311 area stands out for its high dynamic storage and seasonality in recessions. Saturation excess dominates overland flow in the  
312 Coastal plain (Fig. 3f), although evidence for overland flow is weak (Fig. 3e) in contrast to a previous study (Wieczorek and  
313 LaMotte, 2010) that suggests the Florida panhandle has the highest fraction of saturation excess overland flow in the US.

314  
315 In inland areas such as the valleys of the Tennessee-Missouri region, baseflow is moderate and recessions are relatively fast  
316 (Fig. 3a). The Gulf Coast region has lower baseflow and faster, linear recessions. Infiltration excess flow largely occurs in the  
317 narrow ocean margin of the Gulf Coast region but does not extend far inland (Fig. 3f). Exceptions to the area's fast runoff  
318 occur in the Ozark Mountains and the west of the Mississippi embayment where limited areas of high baseflow and slow  
319 recessions occur.

#### 320 4.2.2 Region 2: Midwest and Central

321 The landscape of the Midwest and Central region is dominated by the gradient from recently-glaciated, sandy, forested  
322 watersheds of the Great Lakes region, to the poorly-drained, clay-rich but highly developed for agriculture and populated  
323 region of the Souris-Red-Rainy and Midwest regions. Across the Midwest and Central area, mean watershed elevation ranges  
324 from 200 to 700 meters, and mean annual precipitation varies from 500 to 1,000 mm. Moving west into the Central and  
325 Northern High Plain regions, elevation gradually increases, precipitation decreases, and population density decreases (Fig. S8,  
326 S4, S7). The region experiences mean annual temperatures between 6 to 13°C. The absence of major topographic barriers  
327 results in a continental climate characterized by intense thunderstorms in summer and heavy snowfall in winter.

328  
329 Signature values show that storage capacity is moderate throughout the Midwest (Fig. 3b). Storage in this region is provided  
330 by a moderate snowpack and high depth to bedrock (Fig. S5). Most of the region was previously glaciated, leaving a thick  
331 layer of glacial drift. The soil texture is graded from coarse and sandy around the Great Lakes to clay-rich further South and  
332 West, forming a distinctive outer ring around the Great Lakes region (Miller and White, 1998; Fig. S6). Following this gradient,  
333 there is no significant evidence for overland flow around the Great Lakes, changing to stronger evidence further South-West

334 (Fig. 3e,f). Some occurrence of infiltration excess is consistent with evidence of this process from Midwest agricultural  
335 watersheds (Abban et al., 2014; Davis et al., 2014; Wilson et al., 2012). Streamflow seasonality follows the same gradient (Fig.  
336 3d), with low seasonality around the Great Lakes where sandy aquifers sustain discharge year-round, and higher seasonality  
337 further SouthWest (Miller and White, 1998; Fig. 3d). A second gradient occurs in the MidWest from West to East, following  
338 precipitation and aridity gradients (Fig. S4). In the west, high aridity leads to high water balance losses to ET and low runoff  
339 coefficients at the annual and event scale (Fig. 3c).

#### 340 **4.2.3 Region 3: West and Southwest**

341 The landscape of the West and Southwest region is dominated by the mountain ranges of the Coastal Ranges, Cascades, Sierra  
342 Nevada and Rocky Mountains, with mean watershed elevation ranging from 400 to over 2,700 meters. Dense populations in  
343 the coastal cities give way to sparsely populated inland areas. The climate exhibits strong gradients. The Pacific Northwest  
344 and Sierra Nevada mountain ranges receive substantial amount of precipitation than interior, with mean annual precipitation  
345 ranging from 460 to over 2,100 mm/yr across the region. The region shows a north-south temperature gradient with coastal  
346 moderation. Mean annual temperature ranges from 2°C in northern and high mountain areas to over 20°C in inland southern  
347 desert regions (Fig. S4). Precipitation patterns follow Mediterranean or semi-arid climates characterized by winter precipitation  
348 peaks and dry summers.

349  
350 High baseflows with slow recession are prevalent across most of the Western region, where deep snowpacks drive sustained  
351 baseflow processes (Fig. 3a, S5; Barnhart et al., 2016; Tague and Grant, 2009). Inland areas tend to have faster recessions  
352 while retaining high baseflows, while coastal areas - where snow is rare - have lower baseflow while retaining slow recessions.  
353 The Southwest desert contrasts with the rest of the region, having low baseflows and fast recessions typical of the arid or semi-  
354 arid climate with water tables far below the land surface (Goodrich et al., 1997). Storage capacity and retention follow the  
355 same gradient from high in the Pacific Northwest to low in the South-East, but the high storage region is more constrained to  
356 the Rocky, Cascade and Sierra Nevada mountains (Fig. 3b). Water balance patterns contrast the pattern still further, with only  
357 the high mountains having high runoff ratios in contrast to low ratios throughout the remainder of the Western U.S. (Fig. 3c)  
358 Seasonal variability in processes is higher in the South (primarily California) where the seasonal Mediterranean climate pattern  
359 occurs with hot, dry summers and cool, wet winters (Fig. 3d, S5).

360  
361 Processes in the coastal margin are markedly different from those inland. The moderating influence of the coast is strongly  
362 apparent in storage capacity (Fig. 3b): the northern Coast Ranges have lower average storage compared to high storage inland  
363 areas, while the southern coastal band has higher storage compared to low storage inland areas. Overland flows are strongly  
364 indicated all along the coast, but more weakly inland (Fig. 3c). Most overland flow favors saturation excess, although inland  
365 watersheds of the Southwest desert show areas of infiltration excess (Fig. 3f).

366 **4.3 Inferred climate and landscape drivers of hydrologic processes**

367 In this section, we interpret the random forest models to understand which aspects of climate and landscape are most important  
368 in controlling hydrologic processes in different regions of the U.S. We hypothesize that variable importance statistics from  
369 Shapley and permutation analysis reflect the relative importance of hydrologic process drivers. Random forest models  
370 performed reasonably well ( $R^2 > 0.4$ ) for most signatures (Fig. 5), consistent with previous studies using similar model setups  
371 (Addor et al., 2018; Beck et al., 2015; Bolotin and McMillan, 2024; Kuentz et al., 2017). Performance was higher for baseflow,  
372 water balance loss, and seasonality signatures, but lower for overland flow signatures. Figure S9 presents the regional model  
373 performances for each signature.

374  
375 Figure 6 provides an overview of variable importance results: Figure 6a focuses on spatial patterns, showing the landscape  
376 attribute category that has the strongest contribution to predictions of signatures and processes for each watershed, calculated  
377 using aggregated Shapley values; Figure 6b provides deeper insights into the ranking of landscape attributes, ordered by  
378 permutation importance, for predicting signatures in each region. Figure S10 complements Figure 6a by showing the  
379 importance of landscape attribute categories in each region, based on permutation importance.

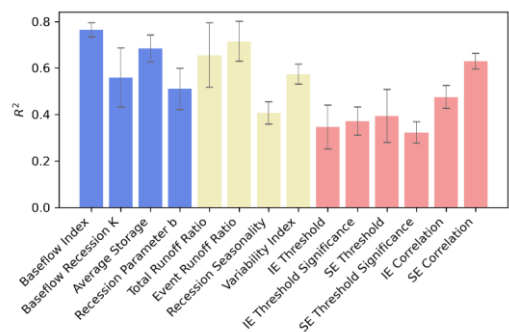
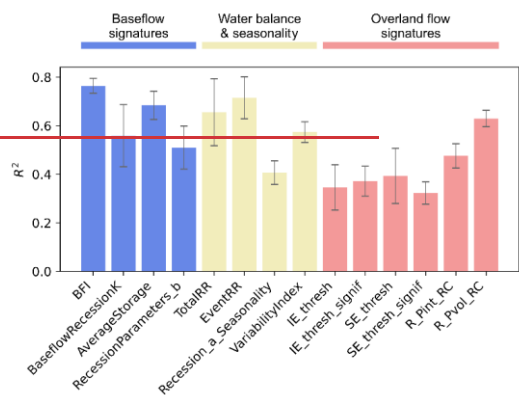
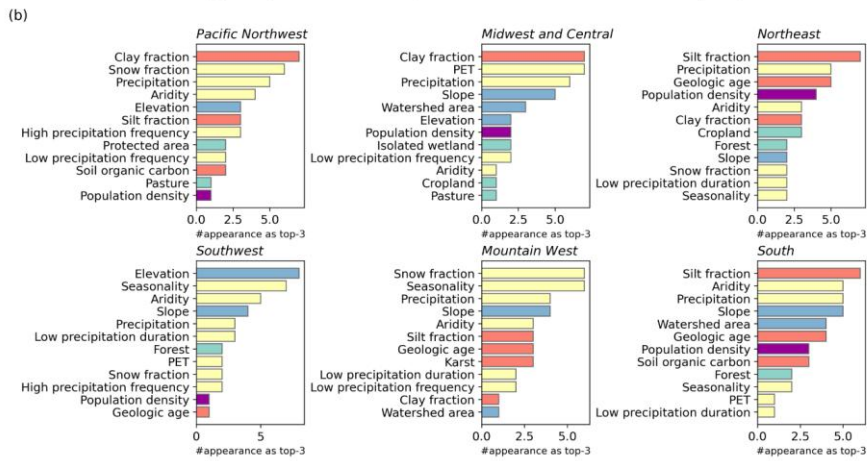
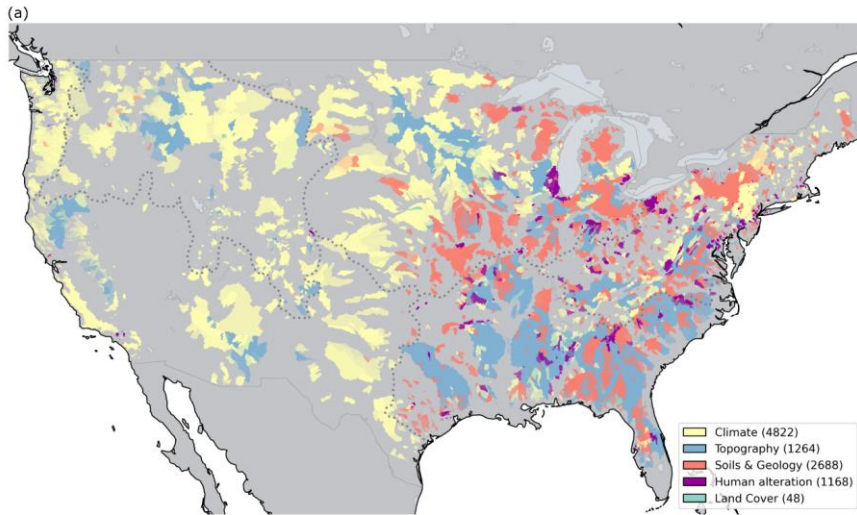
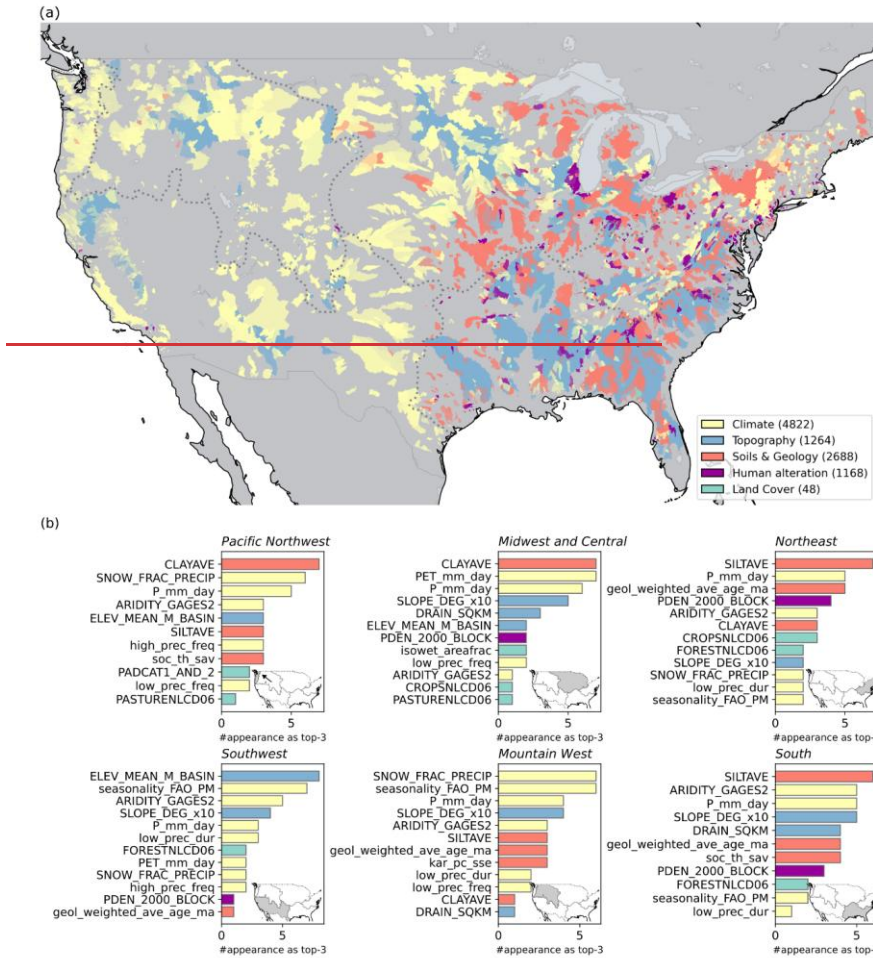


Figure 5: Ten-fold cross-validation performance of the random forest model trained on 4,748 CONUS-samples, where gauge IDs overlapped with Caravan and GAGES-II. Bars show the average  $R^2$  between observed and predicted signatures, with error bars representing the standard deviation. See Table 1 for signature names.





386  
 387 **Figure 6: (a) The landscape attribute category that contributes most to hydrologic responses was identified based on the average**  
 388 **relative contribution of each category,  $\bar{R}_k^{(y,i)}$  (derived from Shapley values; see Section 3.4). For each watershed, the most important**  
 389 **category  $k$  was determined using the median of  $\bar{R}_k^{(y,i)}$  across all hydrologic signatures. Results are displayed for the watershed**  
 390 **samples included in the random forest training. Numbers in the legend indicate the frequency that each category was identified as**  
 391 **the most important. (b) Frequency of watershed attributes ranked among the top three most important variables in permutation**  
 392 **importance (IncMSE%) across all signatures in six U.S. climate regions. The x-axis indicates how many times each attribute**  
 393 **appeared in the top three. See Section 3.4 and Table 2 for attribute names.**

394 **4.3.1 Region 1: East and South**

395 In the East and South, a wide variety of landscape attribute categories dominate process predictions, including topography,  
396 soils and geology, climate and human alteration (Fig. 6). Climate attributes dominate in cooler areas in the Northeast and along  
397 the Appalachian spine, while topography attributes dominate on the Eastern coastal plain. Along the Gulf Coast, either climate  
398 or soils and geology may dominate. Human alteration attributes dominate clusters of watersheds around cities including New  
399 York, Philadelphia, Washington D.C., Raleigh and Atlanta.

400  
401 Overall, and particularly for signatures relating to storage and water balance in the East and South Region (*Total Runoff Ratio,*  
402 *RR seasonality, Event Runoff Ratio, Recession seasonality, Average Storage, Recession Parameter<sub>s-b</sub>*), the random forest  
403 models show that climate drivers are less important than in the rest of the U.S., and soils and geology, topography, and land  
404 cover drivers are more important (Fig. 6, S10). Human influence (population density) is a more important driver here than in  
405 other regions across most signatures, consistent with large areas of high population (Fig. S7). In addition to the major cities,  
406 highly developed areas of Western Florida show anomalous areas of low baseflow, as do developed Piedmont areas (Zimmer  
407 and Gannon, 2018).

408  
409 In the NorthEast, across all signatures, the drivers that most often appeared in the top three controls of random forest  
410 performance were Silt fraction, Precipitation, Geologic Age and Population density — representing the effects of geology,  
411 soils, climate and human development (Fig. 6b). Climate characteristics appear more often for signatures related to water  
412 balance and overland flow. In the South, Silt fraction, Aridity, Precipitation and Slope occur most often, representing gradients  
413 in elevation and soils from the Appalachians to the coastal plain and into Florida (Figs S6, S8).

414 **4.3.2 Region 2: Midwest and Central**

415 In the Midwest and Central area, a wide variety of landscape attribute categories dominate process predictions, including  
416 topography, soils and geology, climate and human alteration, showing strong spatial patterns (Fig. 6). Soils and geology  
417 attributes dominate in the Great Lakes region, and in the arc of clay-rich soils in the High Plains and Midwest regions (Fig.  
418 S6). A mixture of climate and topography attributes dominate in the Souris-Red-Rainy region. Human alteration attributes  
419 dominate in clusters of watersheds around Chicago, Detroit and Cleveland.

420  
421 Overall in the Midwest and Central area, the random forest models show that land cover and topography drivers are more  
422 important than in the rest of the U.S., while climate drivers are less important. Across all signatures, the drivers that most often  
423 appeared in the top three controls of random forest performance were Clay fraction, PET, Precipitation and Slope —  
424 representing the effects of soils, climate and topography (Fig. 6); this is consistent with the gradual variation in signatures'  
425 spatial patterns accompanying gradients in glacial drift and climate in this region, as discussed in 4.2.2. Despite the flat

Formatted: Normal

426 topography of the region, several topographic attributes appear in the top ten, perhaps reflecting the effect of unusual  
427 topographic features such as the driftless area. Land cover metrics (wetland, cropland, pasture) were secondary drivers,  
428 appearing for signatures related to storage and overland flow.

429

430 The impact of climate is spread between multiple drivers: PET, Precipitation, Low precipitation frequency and Aridity. Climate  
431 drivers in the Midwest and Central area show multiple distinct spatial patterns, with aridity and low precipitation metrics  
432 showing an east-west gradient, temperature and PET having a north-south gradient, and precipitation and seasonality having  
433 a Northwest-Southeast gradient (Fig. S4, S5). Thus, each part of the Midwest and Central area has a unique holistic climate  
434 combination. Climate patterns differ distinctly from the NorthEast-Southwest pattern of the soils and land cover.

#### 435 **4.3.3 Region 3: West and Southwest**

436 In the West, climate attributes dominate process predictions across most watersheds in the Pacific Northwest and Mountain  
437 West (Fig. 6a, S5). Some mountain areas have dominant topographic attributes, and topography drivers are more important in  
438 the Southwest region compared to the wider U.S.. Climate properties that appear most often include Snow fraction,  
439 Precipitation, Aridity and Seasonality (Fig. 6b: regions Pacific Northwest, Southwest, Mountain West). These attributes  
440 describe the primary climatic features of the West and Southwest U.S., which are governed by precipitation and aridity  
441 gradients from North to South, and from coasts to inland (Fig. S4). Inland mountain chains influence flow regimes by providing  
442 spring snowmelt and mountain block recharge, among the many influences of topography on hydrologic processes (Gnann et  
443 al., 2025). These controls are demonstrated by the importance of snow fraction alongside topographic attributes, elevation and  
444 slope. Soil control on runoff process is seen by the importance of clay fraction in the Pacific Northwest, reflecting Oregon's  
445 common clay soils (Miller and White, 1998).

## 446 **5 Discussion**

447 This study creates comprehensive maps of hydrologic processes across the contiguous United States by using machine learning  
448 to analyze streamflow signatures and connecting these signatures to dominant watershed processes. The analysis from over  
449 10,000 watersheds shows distinct regional patterns in estimated hydrologic processes and its potential drivers. These process  
450 maps provide novel information for selecting appropriate hydrologic models across large domains and help hydrologists  
451 anticipate how watersheds will respond to environmental changes such as altered climate or land use. In the following sections,  
452 we discuss how these maps provide new benchmarks (Section 5.1), inform hydrologic modelling (Section 5.2), and outline  
453 directions for future work (Section 5.3).

454 **5.1 New benchmark maps of process understanding over large domains**

455 Our results build on previous work to map hydrologic processes and drivers. Our map of baseflow process importance shows  
456 similar patterns to previous studies into baseflow and groundwater contribution to streamflow (Beck et al., 2013; Santhi et al.,  
457 2008; Xie et al., 2024). As with those studies, our approach of using observations and machine learning methods provides finer  
458 detail than can be estimated using statistical interpolation or by hydrologic or climate models. By combining multiple recent  
459 datasets, we increase the number of observations used in our analysis. In our study, we used >10,000 observed watershed data  
460 within CONUS, representing a substantial advancement compared to the >600 to >3000 observation samples used in previous  
461 studies (Addor et al., 2018; Beck et al., 2013, 2015; Janssen and Ameli, 2021; Wu et al., 2021). Our analysis therefore provides  
462 a new benchmark, offering the most comprehensive coverage and highest spatial characterization of hydrologic processes  
463 across the contiguous United States to date. While larger datasets have been analyzed elsewhere, for example, >8,000  
464 watersheds (Santhi et al., 2008), >23,000 watersheds (Xie et al., 2024), those efforts focused exclusively on baseflow index.  
465 Beck et al. (2013) found sometimes differing drivers of baseflow index and recession slope despite their close connection: by  
466 using bivariate plots, we could more clearly highlight regions where patterns of these two signatures diverge. Those areas  
467 include the Pacific Northwest coast with lower baseflow index but slow recessions, and the central high plains with high  
468 baseflow index but fast recessions.

469  
470 Previous studies investigated patterns of overland flow generation across the U.S. using soil maps and rainfall intensity  
471 (Buchanan et al., 2018) streamflow signatures (Wu et al., 2021) and modeling approaches (Wolock, 2003b). Like us, Buchanan  
472 et al. (2018) and Wu et al., (2021) found infiltration excess runoff important throughout the high plains, and saturation excess  
473 in the valleys of the Tennessee-Missouri region, and a mixture of saturation and infiltration excess in the Southwestern U.S..  
474 Substantial overland flow occurs in Southwest chaparral systems (Valeron and Meixner, 2010), and although deep groundwater  
475 tables suggest infiltration excess, we found a mixture of mechanisms. This may reflect vegetation shifting the inferred overland  
476 flow mechanism toward saturation excess. Infiltration excess is inferred when overland flow is related to storm intensity rather  
477 than storm size. In arid and semi-arid catchments, vegetation can locally increase infiltration capacity and soil water retention,  
478 reducing the extent of infiltration excess overland flow (Stein et al., 2021). Additionally, where smaller storms are intercepted  
479 by canopies, signatures may incorrectly attribute the runoff to saturation excess rather than infiltration excess. However, our  
480 results are supported by global studies that show saturation excess is always more common than infiltration excess even in arid  
481 regions, as saturation excess is generated in riparian zones and topographic convergence areas where water tables are higher  
482 (McMillan et al., 2025).

483  
484 By mapping and categorizing the primary drivers of runoff processes, we can untangle which physical characteristics drive the  
485 hydrologic response in each region. In the East and South, soil, geology, and topography emerged as primary drivers, which  
486 is consistent with regional hydrologic process knowledge. Topography is important in the Appalachian Piedmont, where wide

487 and wet valley bottoms generate fast responses (Zimmer and Gannon, 2018). Soils are important along the Gulf Coast where  
488 clay-rich soils promote infiltration-excess overland flow (Miller, 1999; Fig. S6), producing mixed storage and water balance  
489 signatures despite deep bedrock (Fig. S5) and semi-consolidated sand aquifers; and on the Eastern Coastal Plain where sandy  
490 soils, seasonal flooding, and wetlands likely support a single dominant groundwater reservoir supplying baseflow (Fig. 3b;  
491 Holt and McMillan, 2025; Hupp, 2000). The machine learning approach is especially powerful for this purpose, as multiple  
492 landscape attributes often contribute simultaneously to the hydrologic response.

493  
494 Our maps of primary drivers based on Shapley values extend previous work to analyze the drivers of hydrologic signatures.  
495 For example, Addor et al. (2018; their Fig. 3) show that climate (aridity, seasonality, snow fraction) is the primary driver across  
496 most signatures, with topography (elevation, slope) and land cover (forest, leaf area index) being secondary drivers. Figure 6a  
497 similarly shows climate and topography as dominant, but adds spatial information to show that, for example, climate is  
498 dominant in the mountainous western U.S., but soils and geology dominate the Midwest and much of the Northeastern U.S.  
499 Geological age, a recently-proposed attribute to summarize watershed geology, was often in the top random forest attributes  
500 (Holt and McMillan, 2025). This highlights the need and opportunity for development of new landscape attributes that  
501 characterize the subsurface, echoing the call by Tarasova et al. (2023) [and do Nascimento et al., \(2025\)](#).

502  
503 In four of the six regions, soil texture, particularly silt or clay fraction, was identified as a recurring primary driver (Fig. 6b),  
504 though their roles differ by context. In the Northeast, silt dominates variable importance; silt is found in glacial till layer and  
505 supports high water storage and baseflow (Shanley et al., 2015) while facilitating subsurface stormflow under wet conditions  
506 (Detty and McGuire, 2010). In the South, despite silt being identified as a primary driver, clay is the dominant soil texture in  
507 many areas (Miller and White, 1998); in the Mississippi embayment, extensive confining units of clay and silt separate aquifers  
508 and control the groundwater flow (Renken, 1998; Clark et al., 2011). These two cases suggest that Shapley or permutation-  
509 based methods may not fully separate correlated variables due to their treatment of joint variable distributions, and high clay  
510 content may be implicitly captured through the absence of silt in regional analyses.

## 511 **5.2 Informing model selection and evaluation**

512 Our results support hydrological modeling by enabling hydrologists to check whether key processes in a watershed are well-  
513 represented by a candidate model prior to application. A wide range of hydrologic models with differing process  
514 representations, structures and complexities are available (Knoben et al., 2020). Hydrologists must make choices on whether  
515 to include simulations of additional processes such as snowpack or deep groundwater, and the complexity required such as  
516 including energy balance at the land surface. Our maps of hydrologic processes provide a pre-screening tool to match  
517 hydrological models with appropriate process representations to regions. This approach aims to reduce model structural errors  
518 by discouraging use of models ill-suited to the dominant processes (e.g., using a bucket model in overland flow-dominated  
519 regions).

520

521 Many previous studies have assessed preferred model structure in individual research watersheds, often using in-depth data  
522 analysis to ensure that modeled processes are consistent with observed processes (e.g. Hrachowitz et al., 2014; Kavetski and  
523 Fenicia, 2011). This study provides a method to support transparent model justification in applied studies without the resources  
524 to conduct model structure investigations, and to upscale model structure decisions to large domains. For example, if selecting  
525 models from the MARRMoT toolbox (Knoben et al., 2020), models for regions of dominant overland flow should include  
526 saturation excess and/or infiltration excess pathways, and models for regions of complex storage and retention should include  
527 multiple parallel groundwater reservoirs. The ability to choose appropriate models for thousands of watersheds is needed for  
528 new, flexible model frameworks such as the U.S. Next-Generation National Water Model Framework (Cosgrove et al., 2024;  
529 Johnson et al., 2023; Ogden et al., 2021). Our observation-based method complements previous large-domain model-based  
530 methods that use analysis of model sensitivities (Markstrom et al., 2016) and performance (Prieto et al., 2021; Spieler et al.,  
531 2020) Therefore, where hydrologists seek to evaluate models against process representation, this study offers an opportunity  
532 to enhance model benchmarking frameworks by adding process realism as a metric.

### 533 **5.3 Limitations and future work**

534 The hydrologic process maps produced by this study are limited to the contiguous U.S.. Recent streamflow observation datasets  
535 offer the opportunity to extend this method to other regions or globally. Such datasets include the community Caravan dataset  
536 (Kratzert et al., 2023), and the international dataset of watersheds with limited human influences, Reference Observatory of  
537 Basins for International hydrological climate change detection (ROBIN; Turner et al., 2025). If extending the method globally,  
538 caution is advised with scaling, in order to represent different ranges of signature values in different regions. In this study, we  
539 plotted signature values as quantiles based on the U.S. distribution, but other countries may have very different signature  
540 distributions (McMillan et al., 2022). Therefore, watershed processes that are considered important in a U.S. context, may be  
541 considered less important in a global context. Further, some regions of the U.S. are excluded or poorly represented in the  
542 dominant process maps presented in this paper, due to a low spatial coverage of USGS stream gages. For example, there are  
543 significant gaps in the arid southwest where perennial streamflow is rare (Kiang et al., 2013; Krabbenhoft et al., 2022). In such  
544 regions there is a need for alternative process-mapping methods that do not rely on streamflow records.

545

546 Hydrological signatures in this study are long-term averages of the multi-year streamflow dynamics, which may not fully  
547 capture temporal variability in watershed processes. Future studies should account for long-term hydroclimatic changes  
548 (Hobeichi et al., 2022; Gudmundsson et al., 2025), as well as inter-annual variability (Vogel et al., 1994) and seasonal  
549 variations in watershed function (Payn et al., 2012; Gomi et al., 2008). Another complication is that hydrologic signatures are  
550 often confounded by multiple processes (McMillan et al., 2020, 2023), whether driven by natural flow dynamics or impaired  
551 by human activities. For example, water abstraction by reservoirs reduces downstream flow variability and increases water  
552 balance deficits (Salwey et al., 2022; Veldkamp et al., 2016), but changes in vegetation or climate could induce similar effects.

553 Disentangling these impacts remains challenging without testing narrower hypotheses about watershed function, incorporating  
554 expert knowledge, or having detailed information about human interventions. In this study, we partially mitigated this issue  
555 by using multiple signatures to characterize processes, and by representing human alteration through population density, which  
556 showed strong explanatory power for the signatures. Nevertheless, considerable effort is still needed to isolate the combined  
557 impacts of multiple processes, as well as the effects of urban development and agricultural practices on flow dynamics  
558 (Grantham et al., 2022) for improving the large-scale application of signatures.

559 A limitation of this study that would become more apparent at a global scale is the quality of precipitation, streamflow, and  
560 attribute data. A previous study noted issues with limited quality and consistency of the global attribute data for soils and  
561 geology that reduced their predictive power (Beck et al., 2015). Continental scales necessitate the use of gridded precipitation  
562 products, but in areas with low density of observations these products may be insufficient to analyze localized, flashy processes  
563 such as infiltration excess flow (McMillan et al., 2023). In small, headwater watersheds, precipitation grid size may be large  
564 compared to watershed area, and headwaters are also underrepresented in streamflow observations (Golden et al., 2025).  
565 Additionally, errors in watershed boundary delineation would affect signatures that use drainage area to normalize flow, such  
566 as runoff ratio (*Total Runoff Ratio*, *Event Runoff Ratio*) and water balance (*Average Storage*). In snowy areas, signature values  
567 can be compromised because liquid water inputs to the watershed come from snowmelt rather than directly from precipitation.  
568 In our study, we excluded snow-dominated watersheds for signatures related to overland flow, as these require event-scale  
569 surface water input that are particularly affected by frozen or snowmelt conditions. Products such as NLDAS3 (Case et al.,  
570 2025) or surface water inputs considering rain-on-snow and snowmelt (Hammond, 2024; Hammond and Kampf, 2020) may  
571 provide future abilities to estimate overland flow processes in snow areas using estimates of hourly snow accumulation and  
572 melt. While our study used potential evapotranspiration (PET) information in only one signature (*Average Storage*),  
573 uncertainty in PET is a major issue of global datasets and needs to be addressed (Clerc-Schwarzenbach et al., 2024; Destouni  
574 and Zarei, 2024) before this approach can be expanded to a variety of (eco)hydrologic processes.

575  
576 A further limitation is the extent to which continental scale maps of dominant processes can be validated. Large-domain  
577 signature datasets can be evaluated for data quality, for interpolation quality using cross-validation, and compared with  
578 previous datasets. However, it is more difficult to determine how accurately signatures relate to processes over large domains.  
579 Research watersheds offer “ground truth” points at which processes are already well understood (Penna, 2024). Previous  
580 studies used a handful of U.S. critical zone observatory watersheds for evaluation (McMillan et al., 2022). However, the large  
581 number of past and present research watersheds across the globe offer an interesting future opportunity for wider-scale  
582 validation of process mapping techniques (McMillan et al., 2025; Sebestyen et al., 2025). Similarly, validation of process  
583 drivers remains challenging. While Shapley values and permutation importance provide explanatory power for random forest  
584 models, they have some limitations. Both metrics characterize model interactions within a given dataset; therefore, the variety  
585 of processes covered in the dataset matters, and data or model uncertainties may propagate into the interpretations (Husic,  
586 2025). Shapley values do not capture joint distributional effects among multiple interacting variables (Lundberg and Lee,

587 2017). Developing an explanatory framework that maximizes both model performance and interpretability remains an ongoing  
588 research area in hydrology (Robert Maier et al., 2024; Willard et al., 2024).

## 589 6 Conclusion

590 A fundamental question in hydrology is how hydrologic processes are organized over large scales, and how they are controlled  
591 by climate and landscape (Blöschl et al., 2019). In this study, we contribute towards answering this question by mapping  
592 hydrologic processes and their drivers across the contiguous U.S.. Our approach used hydrologic signatures to describe  
593 streamflow dynamics, and connected these dynamics to dominant processes in the associated watersheds using established  
594 relationships between signatures and watershed processes. We analyzed 14,146 gauged U.S. watersheds; our map of processes  
595 was based on observational data from 10,261 gauged sites and extended using random forest predictions to an additional 3,885  
596 watersheds with insufficient record length or completeness. Our method enables knowledge transfer from gauged basins with  
597 well-established conceptual models to ungauged or poorly instrumented watersheds.

599 Our results comprise maps of hydrologic process importance across the contiguous U.S., including baseflow, overland flow,  
600 water storage, seasonal variation and water balance processes. Using interpretable machine learning methods, we create maps  
601 of process drivers that explain which climate and landscape attributes are dominant in controlling hydrologic processes in each  
602 watershed and each region. We find clear patterns at the continental scale in hydrologic processes, with infiltration excess  
603 overland flow dominating the high plains., saturation excess flow prevalent in the valleys of the Tennessee-Missouri region,  
604 and varying baseflow contributions across regions. The novelty of this study is in demonstrating that incorporating more  
605 detailed landscape attribute elucidates non-climate variables as dominant controls on hydrologic processes, even with a large  
606 sample across multiple climate regions. The research further reveals that Specifically, the results showed that climate primarily  
607 controls hydrologic processes in the western U.S., while soils and geology dominate in the Great Lakes region, topography  
608 controls processes in the Southeast, and human influences are most important around large cities across the East. ▲

609  
610 Our findings extend and generalize process understanding from research watersheds to large domains, revealing regional  
611 heterogeneity within broader physiographic provinces that are often treated as hydrologically uniform. Hydrologic process  
612 maps provide essential support for new, large-domain model frameworks that must select model structure across thousands of  
613 watersheds. These maps enable hydrologists to select models that adequately represent the dominant processes of a watershed.  
614 Identification of dominant processes in each region further enables hydrologists to anticipate streamflow response to  
615 environmental change, by identifying which processes are most sensitive to shifts in driving variables. Such analysis has the  
616 potential to support scenario testing for future land use or climate, to guide selection of green and grey infrastructure compatible  
617 with dominant processes, and to inform risk assessments for regions prone to flash flooding, streamflow depletion, or altered  
618 seasonal flow regimes.

Formatted: English (United States)

619 **Code availability**

620 Code used for analysis is available via Zenodo at (*The Zenodo link will be made available following the revision and upon*  
621 *completion of the publication-ready version*) and as a continuously updated version via GitHub at  
622 <https://github.com/RY4GIT/signature-prediction>. Code used to calculate geologic and wetland attributes (Holt and McMillan,  
623 2025) is deposited in Zenodo at (*The Zenodo link will be made available following the revision and upon completion of the*  
624 *publication-ready version*) and as a continuously updated version via GitHub  
625 at [https://github.com/RY4GIT/Wetland\\_GeologicAge\\_Attributes](https://github.com/RY4GIT/Wetland_GeologicAge_Attributes). Caravan attributes for GAGES-II only watersheds were  
626 calculated using <https://github.com/kratzert/Caravan> (Kratzert et al., 2023). Hydrologic signatures are calculated using  
627 <https://github.com/RY4GIT/TOSSH>, which modified the original TOSSH toolbox <https://github.com/TOSSHtoolbox/TOSSH>  
628 (Gnann et al., 2021b).

629 **Data availability**

630 The hydrologic signature datasets, derived from observed data and predicted using random forest models, are deposited at (*The*  
631 *Hydroshare link will be made available following the revision and upon completion of the publication-ready version*). The  
632 Caravan Version 1.5 dataset is available at <https://doi.org/10.5281/zenodo.10968468> (Kratzert et al., 2024), which contains  
633 streamflow, meteorological data, watershed boundaries and attributes. GAGES-II attributes are available at  
634 <https://www.sciencebase.gov/catalog/item/631405bbd34e36012efa304a> (Falcone, 2011), and time series of meteorological  
635 data for GAGES-II locations are available from <https://www.sciencebase.gov/catalog/item/64134069d34eb496d1ce3c6f>  
636 (Wieczorek et al., 2023) and <https://www.sciencebase.gov/catalog/item/6494515fd34ef77fcb014eb0> (Hammond, 2024).  
637 CAMELSH hourly NLDAS forcings are available at <https://doi.org/10.5281/zenodo.15066778> and  
638 <https://doi.org/10.5281/zenodo.15070091> (Tran et al., 2025).

639 **Author contribution**

640 **Araki:** conceptualization, data curation, formal analysis, investigation, methodology, software, visualization, writing —  
641 original draft preparation, writing — review and editing. **Holt:** conceptualization, data curation, methodology, software, writing  
642 — review and editing. **Hammond:** data curation, formal analysis, methodology, writing — original draft preparation, writing  
643 — review and editing. **Husic:** formal analysis, investigation, methodology, writing — original draft preparation, writing —  
644 review and editing. **Coxon:** investigation, writing — review and editing. **McMillan:** funding acquisition, project administration,  
645 conceptualization, formal analysis, investigation, methodology, writing — original draft preparation, writing — review and  
646 editing, supervision.

647 **Competing interests**

648 At least one of the (co-)authors is a member of the editorial board of Hydrology and Earth System Sciences. The peer-review  
649 process was guided by an independent editor, and the authors also have no other competing interests to declare.

650 **Acknowledgement**

651 We thank Sebastian Gnann for the development of the TOSSH toolbox and for the collaborative discussions around my pull  
652 requests, Yueling Ma for helpful input on interpretable Machine Learning methods during a conference, and Andy Wood for  
653 valuable feedback about anthropogenic impacts on streamflow patterns and signatures. The bivariate map was inspired by a  
654 blogpost written by Muhammad Mohsin Raza on their website DataWim. We thank Roy Sando and Scott Hamshaw for helpful  
655 feedback on the earlier version of the manuscript. We appreciate the computing support provided by the IT team at the  
656 Department of Geography, San Diego State University, and the General Research IT (GRIT) team at the University of  
657 California, Santa Barbara. Any use of trade, firm, or product names is for descriptive purposes only and does not imply  
658 endorsement by the U.S. government.

659 **Financial Support**

660 Araki, Holt, McMillan were supported by the NSF Hydrologic Sciences Program, Division of Earth Sciences, Award Number  
661 2124923. Araki acknowledges support from the Shida Scholarship Program. Coxon was supported by a UKRI Future Leaders  
662 Fellowship [MR/V022857/1].

663

665 **Table 1:** Hydrologic signatures used for building process hypotheses. The signature descriptions are adapted from  
 666 (McMillan et al., 2022).

Hydrologic processes and signature hypothesis	Relationship between the signature values and process strength	Signature ( <u>variable name in dataset</u> )	Unit	Description
<b>Baseflow</b>  We hypothesize that a larger baseflow magnitude (i.e., higher <i>Baseflow Index</i> ) and a slower recession rate (i.e., lower <i>Baseflow Recession K</i> ) indicate a stronger baseflow process.	Positive	<i>Baseflow Index (BFI)</i>	-	Baseflow index (BFI) represents baseflow proportion and residence time (Bulygina et al., 2009; Yilmaz et al., 2008). Calculated as mean baseflow divided by mean streamflow. Hydrograph separation is implemented to obtain baseflow fraction using the UKIH smoothed minima method (UKIH, 1980).
	Negative	<i>Baseflow Recession K (Baseflow Recession K)</i>	1/d	Represents groundwater influence and longer subsurface flow paths (Safeeq et al., 2013). Calculated as an exponential recession constant K fitted to the master recession curve derived from adaptive matching strip method.
<b>High storage capacity</b>  We hypothesize that larger storage (i.e., higher <i>Average Storage</i> ) and more nonlinear recession patterns (i.e., higher <i>Recession Parameter s-b</i> ) indicate a greater storage capacity and the involvement of multiple storages.	Positive	<i>Average Storage (Average Storage)</i>	mm	Represents average magnitude of watershed storage (Peters and Aulenbach, 2011). Derived from average baseflow and storage-discharge relationship. Uses a simple water balance model to calculate changes in storage, then finds the relationship between storage and discharge, and then estimates average storage from average baseflow.
	Positive	<i>Recession Parameter b (Recession Parameters b)</i>	-	The nonlinearity indicates the contributions of multiple storages (Clark et al., 2009; Tallaksen, 1995). Recession analysis parameters approximate storage-discharge relationship. Fits a line to the $dQ/dt-Q$ relationship in log-log space for each individual recession and returns the median slope. $b$ is a shape parameter representing the degree of nonlinearity.
<b>Water balance losses</b>  We hypothesize that a smaller runoff ratio (Q:P ratio) at both interannual and event scales (i.e., lower <i>Total Runoff Ratio RR</i> and <i>Event Runoff Ratio RR</i> ) indicates greater water balance losses due to evapotranspiration, deep drainage to groundwater, or some other processes.	Negative	<i>Total Runoff Ratio (Total RR)</i>	-	Total runoff ratio (RR) infer evapotranspiration or other flow bypassing gauge (Safeeq and Hunsaker, 2016). Calculated as mean streamflow divided by mean precipitation.
	Negative	<i>Event Runoff Ratio (Event RR)</i>	-	Event runoff ratio (RR) infer rapid vertical drainage of water to groundwater (Noguchi et al., 1997). Calculated as an average of runoff ratios (streamflow divided by precipitation) from all identified storm events.

<b>Seasonal variability</b>  We hypothesize that greater flow variability, both in general patterns (i.e., higher <i>Variability Index</i> ) and in seasonal patterns (i.e., higher <i>Recession-a-Seasonality</i> ), indicates a stronger influence of seasonal evapotranspiration patterns on water storage.	Positive	<i>Recession Seasonality (Recession_a_Seasonality)</i>	-	Seasonal variation in the recession “a” parameter reflects the impact of evapotranspiration on water storage (Shaw and Riha, 2012). Calculated as the difference between the maximum and minimum monthly median values of the y-intercept (“a” parameter) in the dQ/dt-Q relationship in log-log space, assuming a slope of 2.
	Positive	<i>Variability Index (VariabilityIndex)</i>	-	High variability index shows lower water storage (Estrany et al., 2010). Calculated as the standard deviation of log-transformed discharge values determined at 10% intervals from 10% to 90% of the cumulative frequency distribution (flow duration curve).
<b>Overland flow</b>  We hypothesized that a strong threshold relationship between quickflow and precipitation characteristics (i.e., high significance and higher threshold values) suggests a more dominant overland flow process.	Negative (Values outside the range $0 \leq P\text{-value} \leq 0.05$ are deemed insignificant and clipped out. Within the range, the smaller P-value is, the more significant the threshold is)	<i>Average of IE Threshold Significance (IE_thresh_signif) and IE Threshold Significance (SE_thresh_signif)</i>	-	Significant values ( $<0.05$ ) imply infiltration excess (IE) or saturation excess (SE) occurs (Ali et al., 2013; McGrath et al., 2007). <i>p</i> -value was calculated for the significance of a non-zero change in slope above and below a threshold in a relationship of event quickflow volume versus event maximum precipitation intensity (for IE) or event total precipitation volume (for SE).
	Positive	<i>Average of IE Threshold (IE_thresh) and SE Threshold (SE_thresh)</i>	mm	Indicates rainfall intensity or event precipitation depth required to generate infiltration excess or saturation excess, respectively (Ali et al., 2013; McGrath et al., 2007). Value of the threshold identified in the IE/SE_thresh_signature. The “broken-stick” model was fit to the relationship between quickflow vs. precipitation characteristics.
<b>Overland flow type</b>  We hypothesized that the relative strength in infiltration vs. saturation of excess overland flow (i.e., differences in <i>RC-Pvol-IE Correlation</i> and <i>RC-Pint-SE Correlation</i> ) indicate the prevalence of either overland flow mechanisms.  Exclude watersheds where event runoff coefficient has negative relationships with storm characteristics (i.e., <i>-SE Correlation RC-Pvol</i> < 0 and <i>IE Correlation RC-Pint</i> < 0).	Positive relationship with infiltration excess overland flow	<i>IE Correlation (RC-Pintvol)</i>	-	Indicates stormflow processes sensitive to rainfall intensity, for example, infiltration excess (Hortonian) overland flow (Wu et al., 2021). Calculated as the Spearman correlation coefficients between event runoff coefficient and event maximum rainfall intensity. As per (Wu et al., 2021), event maximum rainfall intensity is calculated as the multiplication of daily rainfall (mm/day) from original climate forcings (i.e., ERA5 for Caravan, gridMET for GAGES-II) multiplied by the fraction of maximum rainfall intensity from CAMELS hourly NLDAS forcings.
	Positive relationship with saturation excess overland flow	<i>SE Correlation (RC-Pvolint)</i>	-	Indicates stormflow processes sensitive to rainfall volume, for example, saturation excess overland flow, subsurface stormflow, and groundwater flow (Wu et al., 2021). Calculated as the Spearman

Formatted: Font: Not Italic

Formatted: Font: Not Italic

Formatted: Font: Italic

Formatted: Font: Italic

				correlation coefficients between event runoff coefficient and rainfall volume.
--	--	--	--	--

667  
668  
669  
670  
671  
672  
673  
674

**Table 2:** Landscape attributes used in training the random forest model. Descriptions are adapted from (Falcone, 2011; Falcone et al., 2010; Holt and McMillan, 2025; Kratzert et al., 2023; Linke et al., 2019). For predictions, when certain attributes are unavailable, equivalent attributes are substituted (e.g., Caravan equivalents are used when predicting signatures for watershed samples available only in Caravan). The combinations are detailed in Table S1. An asterisk (\*) in the unit column indicates that the landscape attribute unit from GAGES-II was converted to the Caravan equivalent (Fig. S11 shows the comparison).

Category	Attribute Name ( <a href="#">variable name in attribute dataset</a> )	Description	Unit	Original Source	Dataset Source	Caravan Equivalent
Physiography	<a href="#">Elevation</a> ( <a href="#">ELEV_MEAN_M_BASIN</a> )	Mean watershed elevation	meters	USGS 100m National Elevation Dataset (Gesch et al., 2018)	GAGES-II	ele_mt_sav
Physiography	<a href="#">Watershed area</a> ( <a href="#">DRAIN_SQKM</a> )	Watershed drainage area	km <sup>2</sup>	Multiple sources, while the majority derived from NHDPlus (U.S. Environmental Protection Agency, 2008) (see original USGS, 2011 report on GAGES-II)	GAGES-II	area
Physiography	<a href="#">Slope</a> ( <a href="#">SLOPE_DEGPCT</a> )	Mean watershed slope, percent	%	USGS 100m resolution National Elevation Dataset (Gesch et al., 2018)	GAGES-II	slp_dg_sav
Land Cover	<a href="#">Forest</a> ( <a href="#">FORESTNLCD06</a> )	Forest extent	% area	NLCD06 for most regions; NLCD01 for Alaska, Hawaii, and Puerto Rico (Yang et al., 2018)	GAGES-II	for_pc_sse
Land Cover	<a href="#">Cropland</a> ( <a href="#">CROPSNLCD06</a> )	Cultivated Crops extent	% area		GAGES-II	crp_pc_sse
Land Cover	<a href="#">Pasture</a> ( <a href="#">PASTURENLCD06</a> )	Pasture/Hay extent	% area		GAGES-II	pst_pc_sse
Land Cover	<a href="#">Irrigated agriculture</a> ( <a href="#">PCT_IRRIG_AG</a> )	Irrigated agriculture extent	% area		GAGES-II	ire_pc_sse
Land Cover	<a href="#">Protected area</a> ( <a href="#">PADCAT1_AND_2</a> )	Percent of watershed	% area *	Protected Areas Database (United States)	GAGES-II	pac_pc_sse

Formatted Table

		designated as Protected Area Category 1 and 2		Geological Survey, 2024)		
Land Cover	<a href="#">Isolated wetland (isowet_areafrac)</a>	Isolated wetland area fraction (Holt, 2024)	-	National Wetlands Inventory (Lane and D'Amico, 2016)	Holt and McMillan, 2025	N/A
Soils & Geology	<a href="#">Clay fraction (CLAYAVE)</a>	Average clay content	%	STATSGO (United States Department of Agriculture et al., 2008)	GAGES-II	cly_pc_sav
Soils & Geology	<a href="#">Silt fraction (SILTAVE)</a>	Average silt content	%		GAGES-II	slt_pc_sav
Soils & Geology	<a href="#">Soil organic carbon (soc_th_sav)</a>	Organic carbon content in soil	tonnes/hectare		Caravan/HydroAtlas	N/A
Soils & Geology	<a href="#">Karst (kar_pc_sse)</a>	Karst area extent	% area	Rock Outcrops v3.0 (Williams and Ford, 2006)	Caravan/HydroAtlas	N/A
Soils & Geology	<a href="#">Geologic age (geol_weighted_average_ma)</a>	Area-weighted average of geologic age	ma	The USGS State Geologic Map Compilation (Horton et al., 2017)	Holt and McMillan, 2025	N/A
Anthropogenic	<a href="#">Population density (PDEN_2000_BLOCK)</a>	Population density in the watershed	persons/km <sup>2</sup>	2000 Census block data regridded to 100m	GAGES-II	ppd_pk_sav
Climate	<a href="#">Precipitation (P_mm_day)</a>	Mean annual precipitation (1971-2000). The unit was converted from the original variable "PPTAVG_BASIN" in cm/year to mm/day.	mm/day *	800m PRISM data	GAGES-II	p_mean
Climate	<a href="#">PET (PET_mm_day)</a>	Mean annual potential evapotranspiration rate estimated from mean monthly air temperature and latitude using Hamon (1961) equation. The unit was converted from the original variable "PET" in	mm/day *	Monthly air temperature from 30-year (1961-1990) PRISM	GAGES-II	pet_mean_FAO_PM

		mm/year to mm/day.				
Climate	<a href="#">Aridity</a> (ARIDITY_GAGES2)	Aridity index, ratio of mean PET and mean precipitation	-	Calculated from PPTAVG BASIN and PET in GAGES-II attributes	GAGES-II	aridity_FAO_PM
Climate	<a href="#">Snow fraction</a> (SNOW_PCT_PRECIP)	Mean snow percent of total precipitation estimate (1901-2000)	- *	McCabe and Wolock (submitted, 2008), 1km grid	GAGES-II	frac_snow
Climate	<a href="#">Seasonality</a> (seasonality_FAO_PM)	Moisture index seasonality in range [0, 2] (Knoben et al., 2018), where 0 indicates no change in the water or energy budget throughout the year, and 2 indicates a transition from fully arid to fully humid conditions. The moisture index is calculated as the normalized aridity index at the monthly scale.	-	ERA-5 (Muñoz Sabater, 2019); The FAO Penman–Monteith equation (Allen et al., 1998; Shalev and Kratzert, 2024) is used to calculate Potential Evapotranspiration (PET)	Caravan/ERA-5	N/A
Climate	<a href="#">High precipitation frequency</a> (high_prec_freq)	Frequency of high precipitation days, where precipitation $\geq 5$ times mean daily precipitation	-	ERA-5 (Muñoz Sabater, 2019)	Caravan/ERA-5	N/A
Climate	<a href="#">Low precipitation frequency</a> (low_prec_freq)	Frequency of low precipitation days, where precipitation $< 1$ mm/day	-	ERA-5 (Muñoz Sabater, 2019)	Caravan/ERA-5	N/A
Climate	<a href="#">Low precipitation duration</a> (low_prec_dur)	Average duration of low precipitation events (number of	day	ERA-5 (Muñoz Sabater, 2019)	Caravan/ERA-5	N/A

		consecutive days where precipitation <1 mm/day)				
--	--	---	--	--	--	--

675 **References**

676 Abban, B., Papanicolaou, A. N. (thanos), Cowles, M. K., and Wilson, C. G.: Examining Seasonal Trends in Sediment Source  
677 Contributions in an Intensely Cultivated Midwestern Sub-Watershed Using Bayesian Unmixing, in: World Environmental and  
678 Water Resources Congress 2014, World Environmental and Water Resources Congress 2014, Portland, Oregon, 1453–1463,  
679 <https://doi.org/10.1061/9780784413548.146>, 2014.

680 Addor, N., Newman, A. J., Mizukami, N., and Clark, M. P.: The CAMELS data set: catchment attributes and meteorology for  
681 large-sample studies, *Hydrol. Earth Syst. Sci.*, 21, 5293–5313, <https://doi.org/10.5194/hess-21-5293-2017>, 2017.

682 Addor, N., Nearing, G., Prieto, C., Newman, A. J., Le Vine, N., and Clark, M. P.: A ranking of hydrological signatures based  
683 on their predictability in space, *Water Resour. Res.*, 54, 8792–8812, <https://doi.org/10.1029/2018WR022606>, 2018.

684 Ali, G., Tetzlaff, D., Soulsby, C., McDonnell, J. J., and Capell, R.: A comparison of similarity indices for catchment  
685 classification using a cross-regional dataset, *Adv. Water Resour.*, 40, 11–22, <https://doi.org/10.1016/j.advwatres.2012.01.008>,  
686 2012.

687 Ali, G., Oswald, C. J., Spence, C., Cammeraat, E. L. H., McGuire, K. J., Meixner, T., and Reaney, S. M.: Towards a unified  
688 threshold-based hydrological theory: necessary components and recurring challenges: INVITED COMMENTARY, *Hydrol.*  
689 *Process.*, 27, 313–318, <https://doi.org/10.1002/hyp.9560>, 2013.

690 Allen, R. G., Pereira, L. S., Raes, D., and Smith, M.: Crop Evapotranspiration – Guidelines for Computing Crop Water  
691 Requirements, in: FAO Irrigation and drainage paper 56, Food and Agriculture Organization of the United Nations, Rome,  
692 Italy, 1998.

693 Almagro, A., Meira Neto, A. A., Vergopolan, N., Roy, T., Troch, P. A., and Oliveira, P. T. S.: The Drivers of Hydrologic  
694 Behavior in Brazil: Insights From a Catchment Classification, *Water Resources Research*, 60,  
695 <https://doi.org/10.1029/2024WR037212>, 2024.

696 Angermann, L., Jackisch, C., Allroggen, N., Sprenger, M., Zehe, E., Tronicke, J., Weiler, M., and Blume, T.: Form and function  
697 in hillslope hydrology: characterization of subsurface flow based on response observations, *Hydrol. Earth Syst. Sci.*, 21, 3727–  
698 3748, <https://doi.org/10.5194/hess-21-3727-2017>, 2017.

699 Araki, R., Branger, F., Wickenkamp, I., and McMillan, H. K.: A signature-based approach to quantify soil moisture dynamics  
700 under contrasting land-uses, *Hydrol. Process.*, 36, e14553, <https://doi.org/10.1002/hyp.14553>, 2022.

701 Ariano, S. and Ali, G.: From river flow regime diversity to proxies for hydrologic homogeneity a Canada-wide case study, *Sci.*  
702 *Rep.*, 15, 16743, <https://doi.org/10.1038/s41598-025-00244-7>, 2025.

703 Arsenault, R., Brissette, F., Martel, J.-L., Troin, M., Lévesque, G., Davidson-Chaput, J., Gonzalez, M. C., Ameli, A., and  
704 Poulin, A.: A comprehensive, multisource database for hydrometeorological modeling of 14,425 North American watersheds,  
705 *Sci Data*, 7, 243, <https://doi.org/10.1038/s41597-020-00583-2>, 2020.

706 Barnhart, T. B., Molotch, N. P., Livneh, B., Harpold, A. A., Knowles, J. F., and Schneider, D.: Snowmelt baseflow  
707 contributions: A comparison of methods using nested catchments in the Colorado River basin, *Water Resources Research*, 52,  
708 4524–4548, 2016.

709 Barnhart, T. B., Farmer, W. H., Hammond, J. C., Sexstone, G. A., Curran, J. H., Koch, J. C., and Driscoll, J. M.: Evaluating  
710 hydrologic region assignment techniques for ungaged basins in Alaska, USA, *River Res. Appl.*, 38, 1569–1584,  
711 <https://doi.org/10.1002/rra.4028>, 2022.

712 Beck, H., Dijk, A., Miralles, D., Jeu, R. A. M., (Sampurno) Bruijnzeel, L., McVicar, T., and Schellekens, J.: Global patterns  
713 in base flow index and recession based on streamflow observations from 3394 catchments, *Water Resources Research*, 49,  
714 7843–7863, <https://doi.org/10.1002/2013WR013918>, 2013.

715 Beck, H. E., De Roo, A., and van Dijk, A. I.: Global maps of streamflow characteristics based on observations from several  
716 thousand catchments, *J. Hydrometeorol.*, 16, 1478–1501, 2015.

717 Bergström, S.: *The HBV Model: Its Structure and Applications*, Swedish Meteorological and Hydrological Institute (SMHI),  
718 Hydrology, Norrköping, 35 pp., 1992.

719 Berghuijs, W. R., Sivapalan, M., Woods, R. A., and Savenije, H. H. G.: Patterns of similarity of seasonal water balances: A  
720 window into streamflow variability over a range of time scales, *Water Resour. Res.*, 50, 5638–5661,  
721 <https://doi.org/10.1002/2014WR015692>, 2014.

722 Blöschl, G.: Hydrologic synthesis: Across processes, places, and scales, *Water Resour. Res.*, 42,  
723 <https://doi.org/10.1029/2005wr004319>, 2006.

724 Blöschl, G., Bierkens, M. F. P., Chambel, A., Cudenneq, C., Destouni, G., Fiori, A., Kirchner, J. W., McDonnell, J. J., Savenije,  
725 H. H. G., Sivapalan, M., Stumpff, C., Toth, E., Volpi, E., Carr, G., Lupton, C., Salinas, J., Széles, B., Viglione, A., Aksoy, H.,  
726 Allen, S. T., Amin, A., Andréassian, V., Arheimer, B., Aryal, S. K., Baker, V., Bardsley, E., Barendrecht, M. H., Bartosova,  
727 A., Batelaan, O., Berghuijs, W. R., Beven, K., Blume, T., Bogaard, T., Borges de Amorim, P., Böttcher, M. E., Boulet, G.,  
728 Breinl, K., Brilly, M., Brocca, L., Buytaert, W., Castellarin, A., Castelletti, A., Chen, X., Chen, Y., Chen, Y., Chiffard, P.,  
729 Claps, P., Clark, M. P., Collins, A. L., Croke, B., Dathe, A., David, P. C., de Barros, F. P. J., de Rooij, G., Di Baldassarre, G.,  
730 Driscoll, J. M., Duethmann, D., Dwivedi, R., Eris, E., Farmer, W. H., Feiccabrino, J., Ferguson, G., Ferrari, E., Ferraris, S.,  
731 Fersch, B., Finger, D., Foglia, L., Fowler, K., Gartsman, B., Gascoïn, S., Gaume, E., Gelfan, A., Geris, J., Gharari, S., Gleeson,  
732 T., Glendell, M., Gonzalez Bevacqua, A., González-Dugo, M. P., Grimaldi, S., Gupta, A. B., Guse, B., Han, D., Hannah, D.,  
733 Harpold, A., Haun, S., Heal, K., Helfricht, K., Herrnegger, M., Hipsey, M., Hlaváčiková, H., Hohmann, C., Holko, L.,  
734 Hopkinson, C., Hrachowitz, M., Illangasekare, T. H., Inam, A., Innocente, C., Istanbuluoglu, E., Jarihani, B., et al.: Twenty-  
735 three unsolved problems in hydrology (UPH) – a community perspective, *Hydrol. Sci. J.*, 64, 1141–1158,  
736 <https://doi.org/10.1080/02626667.2019.1620507>, 2019.

737 Bolotin, L. A. and McMillan, H.: A hydrologic signature approach to analysing wildfire impacts on overland flow, *Hydrol.*  
738 *Process.*, 38, <https://doi.org/10.1002/hyp.15215>, 2024.

739 Bracken, L. J., Wainwright, J., Ali, G. A., Tetzlaff, D., Smith, M. W., Reaney, S. M., and Roy, A. G.: Concepts of hydrological  
740 connectivity: Research approaches, pathways and future agendas, *Earth-Sci. Rev.*, 119, 17–34,  
741 <https://doi.org/10.1016/j.earscirev.2013.02.001>, 2013.

742 Brooks, P. D., Chorover, J., Fan, Y., Godsey, S. E., Maxwell, R. M., McNamara, J. P., and Tague, C.: Hydrological partitioning  
743 in the critical zone: Recent advances and opportunities for developing transferable understanding of water cycle dynamics:  
744 CRITICAL ZONE HYDROLOGY, *Water Resour. Res.*, 51, 6973–6987, <https://doi.org/10.1002/2015wr017039>, 2015.

745 Brunner, M. I., Melsen, L. A., Newman, A. J., Wood, A. W., and Clark, M. P.: Future streamflow regime changes in the United  
746 States: assessment using functional classification, *Hydrol. Earth Syst. Sci.*, 24, 3951–3966, [https://doi.org/10.5194/hess-24-](https://doi.org/10.5194/hess-24-3951-2020)  
747 [3951-2020](https://doi.org/10.5194/hess-24-3951-2020), 2020.

748 Buchanan, B., Auerbach, D. A., Knighton, J., Evensen, D., Fuka, D. R., Easton, Z., Wiczorek, M., Archibald, J. A.,  
749 McWilliams, B., and Walter, T.: Estimating dominant runoff modes across the conterminous United States, *Hydrol. Process.*,  
750 32, 3881–3890, <https://doi.org/10.1002/hyp.13296>, 2018.

751 Bulygina, N., McIntyre, N., and Wheeler, H.: Conditioning rainfall-runoff model parameters for ungauged catchments and  
752 land management impacts analysis, *Hydrol. Earth Syst. Sci.*, 13, 893–904, <https://doi.org/10.5194/hess-13-893-2009>, 2009.

753 Case, J. L., Mocko, D. M., Hain, C. R., Maina, F. Z., Whitney, K. M., Kumar, S. V., Wade, R. A., Locke, K. A., and White,  
754 K. D.: NLDAS-3: Next-Generation Land Data Assimilation System to Support North American Water-Informed Decisions,  
755 in: 2025 National Soil Moisture Workshop, 2025.

756 Clark, M., Rupp, D., Woods, R., Meerveld, H., Peters, N., and Freer, J.: Consistency between hydrological models and field  
757 observations: linking processes at the hillslope scale to hydrological responses at the watershed scale, *Hydrological Processes*,  
758 23, 311–319, <https://doi.org/10.1002/HYP.7154>, 2009.

759 Clark, M., Nijssen, B., Lundquist, J., Kavetski, D., Rupp, D., Woods, R., Freer, J., Gutmann, E., Wood, A., Brekke, L., Arnold,  
760 J., Gochis, D., and Rasmussen, R.: A unified approach for process-based hydrologic modeling: 1. Modeling concept, *Water*  
761 *Resources Research*, 51, 2498–2514, <https://doi.org/10.1002/2015WR017198>, 2015.

762 Clerc-Schwarzenbach, F., Selleri, G., Neri, M., Toth, E., van Meerveld, I., and Seibert, J.: Large-sample hydrology – a few  
763 camels or a whole caravan?, *Hydrol. Earth Syst. Sci.*, 28, 4219–4237, <https://doi.org/10.5194/hess-28-4219-2024>, 2024.

764 Clark, B. R., Hart, R. M., and Gurdak, J.J.: Groundwater Availability of the Mississippi Embayment, U.S. Geological Survey,  
765 Reston, Professional Paper 1785, 62p.

766 Cosgrove, B., Gochis, D., Flowers, T., Dugger, A., Ogden, F., Graziano, T., Clark, E., Cabell, R., Casiday, N., Cui, Z., Eicher,  
767 K., Fall, G., Feng, X., Fitzgerald, K., Frazier, N., George, C., Gibbs, R., Hernandez, L., Johnson, D., Jones, R., Karsten, L.,  
768 Kefelegn, H., Kitzmiller, D., Lee, H., Liu, Y., Mashriqui, H., Mattern, D., McCluskey, A., McCreight, J. L., McDaniel, R.,  
769 Midekisa, A., Newman, A., Pan, L., Pham, C., RafieeiNasab, A., Rasmussen, R., Read, L., Rezaeianzadeh, M., Salas, F., Sang,  
770 D., Sampson, K., Schneider, T., Shi, Q., Sood, G., Wood, A., Wu, W., Yates, D., Yu, W., and Zhang, Y.: NOAA’s National

771 Water Model: Advancing operational hydrology through continental-scale modeling, *J. Am. Water Resour. Assoc.*, 60, 247–  
772 272, <https://doi.org/10.1111/1752-1688.13184>, 2024.

773 Davis, C. A., Ward, A. S., Burgin, A. J., Loecke, T. D., Riveros-Iregui, D. A., Schnoebelen, D. J., Just, C. L., Thomas, S. A.,  
774 Weber, L. J., and St. Clair, M. A.: Antecedent Moisture Controls on Stream Nitrate Flux in an Agricultural Watershed, *Journal*  
775 *of Environmental Quality*, 43, 1494–1503, <https://doi.org/10.2134/jeq2013.11.0438>, 2014.

776 DeCicco, L. A., Hirsch, R. M., Lorenz, D., Watkins, D., and Michael Johnson, J.: dataRetrieval, U.S. Geological Survey,  
777 <https://doi.org/10.5066/P9X4L3GE>, 2018.

778 Destouni, G. and Zarei, M.: Water and climate interplay on land in comparative datasets: Revealing unrealistic major drying  
779 bias of climate reanalysis over Africa and the world, *AGUFM*, 2024, H54B–05, 2024.

780 Dettinger, M. D. and Diaz, H. F.: Global characteristics of stream flow seasonality and variability, *J. Hydrometeorol.*, 1, 289–  
781 310, [https://doi.org/10.1175/1525-7541\(2000\)001<0289:gcsofs>2.0.co;2](https://doi.org/10.1175/1525-7541(2000)001<0289:gcsofs>2.0.co;2), 2000.

782 Detty, J. M. and McGuire, K. J.: Threshold changes in storm runoff generation at a till-mantled headwater catchment, *Water*  
783 *Resour. Res.*, 46, <https://doi.org/10.1029/2009wr008102>, 2010.

784 Dhungel, S., Tarboton, D. G., Jin, J., and Hawkins, C. P.: Potential effects of climate change on ecologically relevant  
785 streamflow regimes: Climate change and streamflow regimes, *River Res. Appl.*, 32, 1827–1840,  
786 <https://doi.org/10.1002/rra.3029>, 2016.

787 Dunne, T.: Field studies of hillslope flow processes, in: Hillslope hydrology, vol. 9, edited by: Kirkby, M. J., John Wiley &  
788 Sons, Inc., 227–293, <https://doi.org/10.18172/cig.1099>, 1978.

789 ▲

790 do Nascimento, T. V., Rudlang, J., Gnann, S., Seibert, J., Hrachowitz, M., & Fenicia, F.: How do geological map details  
791 influence the identification of geology-streamflow relationships in large-sample hydrology studies? *Hydrol. Earth Syst. Sci.*,  
792 29(24), 7173–7200. <https://doi.org/10.5194/hess-29-7173-2025>, 2025.

793 Eng, K. and Wolock, D. M.: Evaluation of machine learning approaches for predicting streamflow metrics across the  
794 conterminous United States, 2022–5058, 2022.

795 Estrany, J., Garcia, C., and Batalla, R. J.: Hydrological response of a small mediterranean agricultural catchment, *J. Hydrol.*  
796 *(Amst.)*, 380, 180–190, <https://doi.org/10.1016/j.jhydrol.2009.10.035>, 2010.

797 Falcone, J.: GAGES-II: Geospatial Attributes of Gages for Evaluating Streamflow, <https://doi.org/10.5066/P96CPHOT>, 2011.

798 Falcone, J. A., Carlisle, D. M., Wolock, D. M., and Meador, M. R.: GAGES: A stream gage database for evaluating natural  
799 and altered flow conditions in the conterminous United States, *Ecology*, 91, 621–621, <https://doi.org/10.1890/09-0889.1>, 2010.

800 Fang, K. and Shen, C.: Full-flow-regime storage-streamflow correlation patterns provide insights into hydrologic functioning  
801 over the continental US, *Water Resour. Res.*, 53, 8064–8083, <https://doi.org/10.1002/2016wr020283>, 2017.

802 Fan, Y., Clark, M., Lawrence, D. M., Swenson, S., Band, L. E., Brantley, S. L., Brooks, P. D., Dietrich, W. E., Flores, A.,  
803 Grant, G., Kirchner, J. W., Mackay, D. S., McDonnell, J. J., Milly, P. C. D., Sullivan, P. L., Tague, C., Ajami, H., Chaney, N.,  
804 Hartmann, A., Hazenberg, P., McNamara, J., Pelletier, J., Perket, J., Rouholahnejad-Freund, E., Wagener, T., Zeng, X.,

Formatted: English (United States)

805 Beighley, E., Buzan, J., Huang, M., Livneh, B., Mohanty, B. P., Nijssen, B., Safeeq, M., Shen, C., Verseveld, W., Volk, J.,  
806 and Yamazaki, D.: Hillslope hydrology in global change research and Earth system modeling, *Water Resour. Res.*, 55, 1737–  
807 1772, <https://doi.org/10.1029/2018wr023903>, 2019.

808 Fenicia, F. and McDonnell, J. J.: Modeling streamflow variability regional scale:(1) perceptual model development through  
809 signature analysis, *Journal Hydrology*, 2022.

810 Frame, J. M., Araki, R., Bhuiyan, S. A., Bindas, T., Rapp, J., Bolotin, L., Deardorff, E., Liu, Q., Haces-Garcia, F., Liao, M.,  
811 Frazier, N., and Ogden, F. L.: Machine learning for a heterogeneous water modeling framework, *J. Am. Water Resour. Assoc.*,  
812 61, <https://doi.org/10.1111/1752-1688.70000>, 2025.

813 Gesch, D. B., Evans, G. A., Oimoen, M. J., and Arundel, S.: The National Elevation Dataset: USGS Earth Resources  
814 Observation and Science Center, 2018.

815 Gnann, S., Baldwin, J. W., Cuthbert, M. O., Gleeson, T., Schwanghart, W., and Wagener, T.: The influence of topography on  
816 the global terrestrial water cycle, *Rev. Geophys.*, 63, e2023RG000810, <https://doi.org/10.1029/2023rg000810>, 2025.

817 Gnann, S. J., Howden, N. J. K., and Woods, R. A.: Hydrological signatures describing the translation of climate seasonality  
818 into streamflow seasonality, *Hydrol. Earth Syst. Sci. Discuss.*, 24, 561–580, <https://doi.org/10.5194/hess-24-561-2020>, 2020.

819 Gnann, S. J., McMillan, H. K., Woods, R. A., and Howden, N. J. K.: Including Regional Knowledge Improves Baseflow  
820 Signature Predictions in Large Sample Hydrology, *Water Resour. Res.*, 57, e2020WR028354,  
821 <https://doi.org/10.1029/2020WR028354>, 2021a.

822 Gnann, S. J., Coxon, G., Woods, R. A., Howden, N. J. K., and McMillan, H. K.: TOSSH: A Toolbox for Streamflow Signatures  
823 in Hydrology, *Environmental Modelling & Software*, 138, 104983, <https://doi.org/10.1016/j.envsoft.2021.104983>, 2021b.

824 Golden, H. E., Christensen, J. R., McMillan, H. K., Kelleher, C. A., Lane, C. R., Husic, A., Li, L., Ward, A. S., Hammond, J.,  
825 Seybold, E. C., Jaeger, K. L., Zimmer, M., Sando, R., Jones, C. N., Segura, C., Mahoney, D. T., Price, A. N., and Cheng, F.:  
826 Advancing the science of headwater streamflow for global water protection, *Nat Water*, 1–11, <https://doi.org/10.1038/s44221-024-00351-1>, 2025.

827

828 Gomi, T., Sidle, R. C., Ueno, M., Miyata, S., & Kosugi, K. (2008). Characteristics of overland flow generation on steep  
829 forested hillslopes of central Japan. *Journal of Hydrology*, 361(3-4), 275-290.  
830 <https://doi.org/10.1016/j.jhydrol.2008.07.045>

831 Goodrich, D. C., Lane, L. J., Shillito, R. M., Miller, S. N., Syed, K. H., and  
832 Woolhiser, D. A.: Linearity of basin response as a function of scale in a semiarid watershed, *Water Resour. Res.*, 33, 2951–  
2965, <https://doi.org/10.1029/97wr01422>, 1997.

833 Grantham, T. E., Carlisle, D. M., Howard, J., Lane, B., Lusardi, R., Obester, A., Sandoval-Solis, S., Stanford, B., Stein, E. D.,  
834 Taniguchi-Quan, K. T., Yarnell, S. M., and Zimmerman, J. K. H.: Modeling functional flows in California’s rivers, *Front.*  
835 *Environ. Sci.*, 10, <https://doi.org/10.3389/fenvs.2022.787473>, 2022.

836 Gudmundsson, L., Brunner, M. I., Döll, P., Fluet-Chouinard, E., Frolova, N., Gosling, S. N., Hirabayashi, Y., Kireeva, M. B.,  
837 Liu, X., Müller Schmied, H., Magritskiy, D., Slater, L. J., Stein, L., Trambly, Y., Wang, K., Wasko, C., Yamazaki, D., and

838 Zhou, X.: Past and future change in global river flows, *Nat. Rev. Earth Environ.*, <https://doi.org/10.1038/s43017-025-00745->  
839 [z](https://doi.org/10.1038/s43017-025-00745-z), 2025.

840 Haines, A., Finlayson, B., and McMahon, T.: A global classification of river regimes, *Applied Geography*, 8, 255–272,  
841 [https://doi.org/10.1016/0143-6228\(88\)90035-5](https://doi.org/10.1016/0143-6228(88)90035-5), 1988.

842 Hammond, J. C.: Daily time series of surface water input from rainfall, rain on snow, and snowmelt for the Conterminous  
843 United States from 1990 to 2023, as well as annual series of input seasonality, precipitation seasonality, and average rainfall,  
844 rain on snow, and snowmelt rates, <https://doi.org/10.5066/P9JWJPNC>, 2024.

845 Hammond, J. C. and Kampf, S. K.: Subannual streamflow responses to rainfall and snowmelt inputs in snow-dominated  
846 watersheds of the western United States, *Water Resour. Res.*, 56, <https://doi.org/10.1029/2019wr026132>, 2020.

847 Hammond, J. C., Zimmer, M., Shanafield, M., Kaiser, K., Godsey, S. E., Mims, M. C., Zipper, S. C., Burrows, R. M., Kampf,  
848 S. K., Dodds, W., Jones, C. N., Krabbenhoft, C. A., Boersma, K. S., Datry, T., Olden, J. D., Allen, G. H., Price, A. N., Costigan,  
849 K., Hale, R., Ward, A. S., and Allen, D. C.: Spatial patterns and drivers of nonperennial flow regimes in the contiguous United  
850 States, *Geophys. Res. Lett.*, 48, <https://doi.org/10.1029/2020gl090794>, 2021.

851 Hammond, J. C., Sexstone, G. A., Putman, A. L., Barnhart, T. B., Rey, D. M., Driscoll, J. M., Liston, G. E., Rasmussen, K. L.,  
852 McGrath, D., Fassnacht, S. R., and Kampf, S. K.: High resolution SnowModel simulations reveal future elevation-dependent  
853 snow loss and earlier, flashier surface water input for the upper Colorado river basin, *Earths Future*, 11,  
854 <https://doi.org/10.1029/2022ef003092>, 2023.

855 Hay, L. E., LaFontaine, J. H., Van Beusekom, A. E., Norton, P. A., Farmer, W. H., Regan, R. S., Markstrom, S. L., and  
856 Dickinson, J. E.: Parameter estimation at the conterminous United States scale and streamflow routing enhancements for the  
857 National Hydrologic Model infrastructure application of the Precipitation-Runoff Modeling System (NHM-PRMS),  
858 <https://doi.org/10.3133/tm6b10>, 2023.

859 Hobeichi, S., Abramowitz, G., Ukkola, A. M., De Kauwe, M., Pitman, A., Evans, J. P., and Beck, H.: Reconciling historical  
860 changes in the hydrological cycle over land, *Npj Clim. Atmos. Sci.*, 5, 17, <https://doi.org/10.1038/s41612-022-00240-y>,  
861 2022.Hodgkins, G. A., Renard, B., Whitfield, P. H., Laaha, G., Stahl, K., Hannaford, J., Burn, D. H., Westra, S., Fleig, A. K.,  
862 Araújo Lopes, W. T., Murphy, C., Mediero, L., and Hanel, M.: Climate driven trends in historical extreme low streamflows  
863 on four continents, *Water Resour. Res.*, 60, <https://doi.org/10.1029/2022wr034326>, 2024.

864 Holt, A.: New Predictors for Hydrologic Signatures: Wetlands and Geologic Age Across Continental Scales, San Diego State  
865 University, United States -- California, 2024.

866 Holt, A. and McMillan, H.: New predictors for hydrologic signatures: Wetlands and geologic age across continental scales,  
867 *Hydrol. Process.*, 39, <https://doi.org/10.1002/hyp.70080>, 2025.

868 Horton, J. D., San Juan, C. A., and Stoesser, D. B.: The State Geologic Map Compilation (SGMC) geodatabase of the  
869 conterminous United States, <https://doi.org/10.3133/ds1052>, 2017.

870 Hrachowitz, M., Fovet, O., Ruiz, L., Euser, T., Gharari, S., Nijzink, R., Freer, J., Savenije, H. H. G., and Gascuel-Oudou, C.:  
871 Process consistency in models: The importance of system signatures, expert knowledge, and process complexity, *Water Resour.*  
872 *Res.*, 50, 7445–7469, <https://doi.org/10.1002/2014wr015484>, 2014.

873 Hupp, C. R.: Hydrology, geomorphology and vegetation of Coastal Plain rivers in the south-eastern USA. *Hydrological*  
874 *processes*, 14, 2991–3010, 2000.

875 Husic, A.: Game theory for catchment science, *ESS Open Archive*, <https://doi.org/10.22541/essoar.173924202.27840286/v1>,  
876 2025.

877 Husic, A., Hammond, J., Price, A. N., and Roundy, J. K.: Interrogating process deficiencies in large-scale hydrologic models  
878 with interpretable machine learning, *Hydrol. Earth Syst. Sci.*, 29, 4457–4472, <https://doi.org/10.5194/hess-29-4457-2025>,  
879 2025.

880 Jackisch, C., Angermann, L., Allroggen, N., Sprenger, M., Blume, T., Tronicke, J., and Zehe, E.: Form and function in hillslope  
881 hydrology: in situ imaging and characterization of flow-relevant structures, *Hydrol. Earth Syst. Sci.*, 21, 3749–3775, 2017.

882 Janssen, J. and Ameli, A. A.: A hydrologic functional approach for improving large-sample hydrology performance in poorly  
883 gauged regions, *Water Resour. Res.*, 57, <https://doi.org/10.1029/2021wr030263>, 2021.

884 Jefferson, A., Grant, G. E., Lewis, S. L., and Lancaster, S. T.: Coevolution of hydrology and topography on a basalt landscape  
885 in the Oregon Cascade Range, USA, *Earth Surf. Process.*, <https://doi.org/10.1002/esp.1976>, 2010.

886 Ji, H., Song, Y., Bindas, T., Shen, C., Yang, Y., Pan, M., Liu, J., Rahmani, F., Abbas, A., Beck, H., Lawson, K., and Wada,  
887 Y.: Distinct hydrologic response patterns and trends worldwide revealed by physics-embedded learning, *arXiv [physics.geo-*  
888 *ph]*, arXiv, 2025.

889 Johnson, J. M., Fang, S., Sankarasubramanian, A., Rad, A. M., Kindl da Cunha, L., Jennings, K. S., Clarke, K. C., Mazrooci,  
890 A., and Yeghiazarian, L.: Comprehensive analysis of the NOAA National Water Model: A call for heterogeneous formulations  
891 and diagnostic model selection, *J. Geophys. Res.*, 128, <https://doi.org/10.1029/2023jd038534>, 2023.

892 Kavetski, D. and Fenicia, F.: Elements of a flexible approach for conceptual hydrological modeling: 2. Application and  
893 experimental insights, *Water Resour. Res.*, 47, <https://doi.org/10.1029/2011wr010748>, 2011.

894 Kennard, M. J., Pusey, B. J., Olden, J. D., Mackay, S. J., Stein, J. L., and Marsh, N.: Classification of natural flow regimes in  
895 Australia to support environmental flow management: Classification of natural flow regimes in Australia, *Freshw. Biol.*, 55,  
896 171–193, <https://doi.org/10.1111/j.1365-2427.2009.02307.x>, 2010.

897 Kiang, J. E., Stewart, D. W., Archfield, S. A., Osborne, E. B., and Eng, K.: A national streamflow network gap analysis (No.  
898 2013-5013), US Geological Survey, 2013.

899 Kirchner, J. W.: Catchments as simple dynamical systems: Catchment characterization, rainfall-runoff modeling, and doing  
900 hydrology backward. *Water Resources Research*, 45(2). <https://doi.org/10.1029/2008WR006912>. 2009.

901 Knoben, W. J. M., Woods, R. A., and Freer, J. E.: A quantitative hydrological climate classification evaluated with independent  
902 streamflow data, *Water Resour. Res.*, 54, 5088–5109, <https://doi.org/10.1029/2018wr022913>, 2018.

903 Knobon, W. J. M., Freer, J. E., Peel, M. C., Fowler, K. J. A., and Woods, R. A.: A brief analysis of conceptual model structure  
904 uncertainty using 36 models and 559 catchments, *Water Resour. Res.*, 56, e2019WR025975,  
905 <https://doi.org/10.1029/2019wr025975>, 2020.

906 Krabbenhoft, C. A., Allen, G. H., Lin, P., Godsey, S. E., Allen, D. C., Burrows, R. M., DelVecchia, A. G., Fritz, K. M.,  
907 Shanafield, M., Burgin, A. J., Zimmer, M. A., Datry, T., Dodds, W. K., Jones, C. N., Mims, M. C., Franklin, C., Hammond, J.  
908 C., Zipper, S., Ward, A. S., Costigan, K. H., Beck, H. E., and Olden, J. D.: Assessing placement bias of the global river gauge  
909 network, *Nat. Sustain.*, 5, 586–592, <https://doi.org/10.1038/s41893-022-00873-0>, 2022.

910 Kratzert, F., Nearing, G., Addor, N., Erickson, T., Gauch, M., Gilon, O., Gudmundsson, L., Hassidim, A., Klotz, D., Nevo, S.,  
911 Shalev, G., and Matias, Y.: Caravan - A global community dataset for large-sample hydrology, *Sci Data*, 10, 61,  
912 <https://doi.org/10.1038/s41597-023-01975-w>, 2023.

913 Kratzert, F., Nearing, G., Addor, N., Erickson, T., Gauch, M., Gilon, O., Gudmundsson, L., Hassidim, A., Klotz, D., Nevo, S.,  
914 Shalev, G., and Matias, Y.: Caravan - A global community dataset for large-sample hydrology Version 1.4,  
915 <https://doi.org/10.5281/ZENODO.10968468>, 2024.

916 Kuentz, A., Arheimer, B., Hundecha, Y., and Wagener, T.: Understanding hydrologic variability across Europe through  
917 catchment classification, *Hydrol. Earth Syst. Sci.*, 21, 2863–2879, 2017.

918 Kuhn, M.: Building predictive models in R using the caret package, *Journal of Statistical Software*, 28, 1–26,  
919 <https://doi.org/10.18637/JSS.V028.I05>, 2008.

920 Lane, B. A., Dahlke, H. E., Pasternack, G. B., and Sandoval-Solis, S.: Revealing the Diversity of Natural Hydrologic Regimes  
921 in California with Relevance for Environmental Flows Applications, *J. Am. Water Resour. Assoc.*, 53, 411–430,  
922 <https://doi.org/10.1111/1752-1688.12504>, 2017.

923 Lane, C. R. and D’Amico, E.: Identification of putative geographically isolated wetlands of the conterminous United States, *J.*  
924 *Am. Water Resour. Assoc.*, 52, 705–722, <https://doi.org/10.1111/1752-1688.12421>, 2016.

925 Lapides, D. A., Zipper, S., and Hammond, J. C.: Identifying hydrologic signatures associated with streamflow depletion caused  
926 by groundwater pumping, *Hydrol. Process.*, 37, <https://doi.org/10.1002/hyp.14877>, 2023.

927 Lee, D., Ward, P., and Block, P.: Defining high-flow seasons using temporal streamflow patterns from a global model, *Hydrol.*  
928 *Earth Syst. Sci.*, 19, 4689–4705, <https://doi.org/10.5194/hess-19-4689-2015>, 2015.

929 Linke, S., Lehner, B., Ouellet Dallaire, C., Ariwi, J., Grill, G., Anand, M., Beames, P., Burchard-Levine, V., Maxwell, S.,  
930 Moidu, H., Tan, F., and Thieme, M.: Global hydro-environmental sub-basin and river reach characteristics at high spatial  
931 resolution, *Sci Data*, 6, 283, <https://doi.org/10.1038/s41597-019-0300-6>, 2019.

932 Lins, H. F.: Regional streamflow regimes and hydroclimatology of the United States, *Water Resour. Res.*, 33, 1655–1667,  
933 <https://doi.org/10.1029/97WR00615>, 1997.

934 Lohse, K. A. and Dietrich, W. E.: Contrasting effects of soil development on hydrological properties and flow paths, *Water*  
935 *Resour. Res.*, 41, <https://doi.org/10.1029/2004wr003403>, 2005.

936 Lundberg, S. and Lee, S.-I.: A unified approach to interpreting model predictions, *arXiv [cs.AI]*, arXiv, 2017.

937 Lundberg, S. M., Erion, G. G., and Lee, S.-I.: Consistent individualized feature attribution for tree ensembles, arXiv [cs.LG],  
938 arXiv, 2018.

939 Markstrom, S. L., Hay, L. E., and Clark, M. P.: Towards simplification of hydrologic modeling: identification of dominant  
940 processes, *Hydrol. Earth Syst. Sci.*, 20, 4655–4671, <https://doi.org/10.5194/hess-20-4655-2016>, 2016.

941 Mazvimavi, D., Meijerink, A. M. J., Savenije, H. H. G., and Stein, A.: Prediction of flow characteristics using multiple  
942 regression and neural networks: A case study in Zimbabwe, *Phys. Chem. Earth (2002)*, 30, 639–647,  
943 <https://doi.org/10.1016/j.pce.2005.08.003>, 2005.

944 McGrath, G. S., Hinz, C., and Sivapalan, M.: Temporal dynamics of hydrological threshold events, *Hydrol. Earth Syst. Sci.*,  
945 11, 923–938, <https://doi.org/10.5194/hess-11-923-2007>, 2007.

946 McMillan, H.: Linking hydrologic signatures to hydrologic processes: A Review, *Hydrol. Process.*, 34, 1393–1409,  
947 <https://doi.org/10.1002/hyp.13632>, 2020.

948 McMillan, H., Gueguen, M., Grimon, E., Woods, R., Clark, M., and Rupp, D. E.: Spatial variability of hydrological processes  
949 and model structure diagnostics in a 50 km<sup>2</sup> catchment, *Hydrol. Process.*, 28, 4896–4913, <https://doi.org/10.1002/hyp.9988>,  
950 2014.

951 McMillan, H., Westerberg, I., and Branger, F.: Five guidelines for selecting hydrological signatures, *Hydrol. Process.*, 31,  
952 4757–4761, <https://doi.org/10.1002/hyp.11300>, 2017.

953 McMillan, H., Araki, R., Bolotin, L., Kim, D.-H., Coxon, G., Clark, M., and Seibert, J.: Global patterns in observed hydrologic  
954 processes, *Nat Water*, <https://doi.org/10.1038/s44221-025-00407-w>, 2025.

955 McMillan, H. K.: A review of hydrologic signatures and their applications, *WIREs Water*, 8, <https://doi.org/10.1002/wat2.1499>,  
956 2021.

957 McMillan, H. K., Gnann, S. J., and Araki, R.: Large scale evaluation of relationships between hydrologic signatures and  
958 processes, *Water Resour. Res.*, 58, <https://doi.org/10.1029/2021wr031751>, 2022.

959 McMillan, H., Coxon, G., Araki, R., Salwey, S., Kelleher, C., Zheng, Y., Knoben, W., Gnann, S., Seibert, J., and Bolotin, L.:  
960 When good signatures go bad: Applying hydrologic signatures in large sample studies, *Hydrol. Process.*, 37,  
961 <https://doi.org/10.1002/hyp.14987>, 2023.

962 McMillan, H. K., Coxon, G., Araki, R., Salwey, S., Kelleher, C., Zheng, Y., Knoben, W., Gnann, S., Seibert, J., and Bolotin,  
963 L.: When good signatures go bad: Applying hydrologic signatures in large sample studies, *Hydrol. Process.*, 37,  
964 <https://doi.org/10.1002/hyp.14987>, 2023.

965 Miller, D. A. and White, R. A.: A conterminous United States multilayer soil characteristics dataset for regional climate and  
966 hydrology modeling, *Earth Interact.*, 2, 1–26, [https://doi.org/10.1175/1087-3562\(1998\)002<0001:acusms>2.3.co;2](https://doi.org/10.1175/1087-3562(1998)002<0001:acusms>2.3.co;2), 1998.

967 Miller, J. A.: Ground water atlas of the United States: Introduction and national summary (No. 730-A), A1–A15, 1999.

968 Molnar, C., Bischl, B., and Casalicchio, G.: iml: An R package for Interpretable Machine Learning,  
969 <https://doi.org/10.21105/joss.00786>, 2018.

970 Miller, D. A. and White, R. A.: A conterminous United States multilayer soil characteristics dataset for regional climate and  
971 hydrology modeling, *Earth Interact.*, 2, 1–26, [https://doi.org/10.1175/1087-3562\(1998\)002%3C0001:acusms%3E2.3.co;2](https://doi.org/10.1175/1087-3562(1998)002%3C0001:acusms%3E2.3.co;2),  
972 1998.

973 Mosley, M. P.: Delimitation of New Zealand hydrologic regions, *J. Hydrol. (Amst.)*, 49, 173–192,  
974 [https://doi.org/10.1016/0022-1694\(81\)90211-0](https://doi.org/10.1016/0022-1694(81)90211-0), 1981.

975 Muñoz Sabater, J.: ERA5-Land monthly averaged data from 1950 to present, <https://doi.org/10.24381/CDS.68D2BB30>, 2019.

976 Neff, B. P., Day, S. M., Piggott, A. R., and Fuller, L. M.: Base flow in the Great Lakes Basin,  
977 <https://doi.org/10.3133/sir20055217>, 2005.

978 Noguchi, S., Nik, A. R., Yusop, Z., Tani, M., and Sammori, T.: Rainfall-runoff responses and roles of soil moisture variations  
979 to the response in tropical Rain Forest, Bukit Tarek, peninsular Malaysia, *J. Forest Res.*, 2, 125–132,  
980 <https://doi.org/10.1007/bf02348209>, 1997.

981 Ogden, F., Avant, B., Bartel, R., Blodgett, D., Clark, E., Coon, E., Cosgrove, B., Cui, S., Kindl da Cunha, L., Farthing, M.,  
982 Flowers, T., Frame, J., Frazier, N., Graziano, T., Gutenson, J., Johnson, D., McDaniel, R., Moulton, J., Loney, D., Peckham,  
983 S., Mattern, D., Jennings, K., Williamson, M., Savant, G., Tubbs, C., Garrett, J., Wood, A., and Johnson, J.: The Next  
984 Generation Water Resources Modeling Framework: Open Source, Standards Based, Community Accessible, Model  
985 Interoperability for Large Scale Water Prediction, AGU Fall Meeting Abstracts, New Orleans, LA, 2021, H43D–01, 2021.

986 Omernik, J. M.: Ecoregions of the conterminous United States, *Ann. Assoc. Am. Geogr.*, 77, 118–125, 1987.

987 Omernik, J. M.: Perspectives on the nature and definition of ecological regions, *Environ. Manage.*, 34 Suppl 1, S27–38,  
988 <https://doi.org/10.1007/s00267-003-5197-2>, 2004.

989 Oswald, C. J., Kelleher, C., Ledford, S. H., Hopkins, K. G., Sytsma, A., Tetzlaff, D., Toran, L., and Voter, C.: Integrating  
990 urban water fluxes and moving beyond impervious surface cover: A review, *J. Hydrol. (Amst.)*, 618, 129188,  
991 <https://doi.org/10.1016/j.jhydrol.2023.129188>, 2023.

992 Oudin, L., Andréassian, V., Perrin, C., Michel, C., and Le Moine, N.: Spatial proximity, physical similarity, regression and  
993 ungauged catchments: A comparison of regionalization approaches based on 913 French catchments, *Water Resources Research*,  
994 44, <https://doi.org/10.1029/2007WR006240>, 2008.

995 Paola, C., Foufoula-Georgiou, E., Dietrich, W. E., Hondzo, M., Mohrig, D., Parker, G., Power, M. E., Rodriguez-Iturbe, I.,  
996 Veldkamp, T. I. E., Wada, Y., Aerts, J. C. J. H., Döll, P., Gosling, S. N., Liu, J., Masaki, Y., Oki, T., Ostberg, S., Pokhrel, Y.,  
997 Satoh, Y., Kim, H., and Ward, P. J.: Water scarcity hotspots travel downstream due to human interventions in the 20th and  
998 21st century, *Nat. Commun.*, 8, 15697, <https://doi.org/10.1038/ncomms15697>, 2017.

999 Vogel, R. M., Member, J., and Asce, N. M.: Flow-duration curves. I: New interpretation and confidence intervals, [https://bpb-](https://bpb-us-e1.wpmucdn.com/sites.tufts.edu/dist/a/4406/files/2019/04/flowDuration1.pdf)  
1000 [us-e1.wpmucdn.com/sites.tufts.edu/dist/a/4406/files/2019/04/flowDuration1.pdf](https://bpb-us-e1.wpmucdn.com/sites.tufts.edu/dist/a/4406/files/2019/04/flowDuration1.pdf).

1001 Voller, V., and Wilcock, P.: Toward a unified science of the Earth’s surface: Opportunities for synthesis among hydrology,  
1002 geomorphology, geochemistry, and ecology, *Water Resour. Res.*, 42, <https://doi.org/10.1029/2005wr004336>, 2006.

1003 Payn, R. A., Gooseff, M. N., and McGlynn, B. L.: Exploring changes in the spatial distribution of stream baseflow generation  
1004 during a seasonal recession, <https://doi.org/10.1029/2011WR011552>, 2012.

1005 Pechlivanidis, I. G. and Arheimer, B.: Large-scale hydrological modelling by using modified PUB recommendations: the  
1006 India-HYPE case, *Hydrol. Earth Syst. Sci.*, 19, 4559–4579, <https://doi.org/10.5194/hess-19-4559-2015>, 2015.

1007 Pedregosa, F., Varoquaux, G., Gramfort, A., Michel, V., Thirion, B., Grisel, O., Blondel, M., Prettenhofer, P., Weiss, R.,  
1008 Dubourg, V., Vanderplas, J., Passos, A., Cournapeau, D., Brucher, M., Perrot, M., and Duchesnay, E.: Scikit-learn: Machine  
1009 Learning in Python, *Journal of Machine Learning Research*, 12, 2825–2830, 2011.

1010 Penna, D.: A recipe for why and how to set up and sustain an experimental catchment, *Hydrol. Process.*, 38,  
1011 <https://doi.org/10.1002/hyp.15163>, 2024.

1012 Peters, N. E. and Aulenbach, B. T.: Water storage at the Panola mountain research watershed, Georgia, USA: Water storage  
1013 at pmrw, *Hydrol. Process.*, 25, 3878–3889, <https://doi.org/10.1002/hyp.8334>, 2011.

1014 Pfister, L., Martínez-Carreras, N., Hissler, C., Klaus, J., Carrer, G. E., Stewart, M. K., and McDonnell, J. J.: Bedrock geology  
1015 controls on catchment storage, mixing, and release: A comparative analysis of 16 nested catchments, *Hydrological Processes*,  
1016 31, 1828–1845, <https://doi.org/10.1002/hyp.11134>, 2017.

1017 Prieto, C., Kavetski, D., Le Vine, N., Álvarez, C., and Medina, R.: Identification of dominant hydrological mechanisms using  
1018 Bayesian inference, multiple statistical hypothesis testing, and flexible models, *Water Resour. Res.*, 57,  
1019 <https://doi.org/10.1029/2020wr028338>, 2021.

1020 Qi, S. L. and Mason, C. A.: Data used to prioritize the selection of river basins for intensive monitoring and assessment by the  
1021 U.S. Geological Survey, <https://doi.org/10.5066/P98194QR>, 2023.

1022 R Core Team (2024). R: A Language and Environment for Statistical Computing. R Foundation for Statistical Computing,  
1023 Vienna, Austria. <https://www.R-project.org/>.

1024 Reinecke, R., Stein, L., Gnann, S., Andersson, J. C. M., Arheimer, B., Bierkens, M., Bonetti, S., Güntner, Kollet, S., Mishra,  
1025 S., Moosdorf, N., Nazari, S., Pokhrel, Y., Prudhomme, C., Schewe, J., Shen, C., and Wagener, T.: Uncertainties guide global  
1026 water model advancement, *WIREs Water*, 12, <https://doi.org/10.1002/wat2.70025>, 2025.

1027 Renken, R. A.: Ground Water Atlas of the United States: Segment 5, Arkansas, Louisiana, Mississippi, Hydrologic Atlas 730,  
1028 28p., U.S. Geological Survey, <https://doi.org/10.3133/ha730F>, 1998.

1029 Robert Maier, H., Rosa Taghikhah, F., Nabavi, E., Razavi, S., Gupta, H., Wu, W., Radford, D. A. G., and Huang, J.: How  
1030 much X is in XAI: Responsible use of “Explainable” artificial intelligence in hydrology and water resources, *J. Hydrol. X*, 25,  
1031 100185, <https://doi.org/10.1016/j.hydroa.2024.100185>, 2024.

1032 Rudlang, J. M., do Nascimento, T. V. M., van der Ent, R., Fencia, F., and Hrachowitz, M.: Climate and landscape jointly  
1033 control Europe's hydrology, *EGUsphere* [preprint], <https://doi.org/10.5194/egusphere-2025-6372>, 2025.

1034 Safeeq, M. and Hunsaker, C. T.: Characterizing runoff and water yield for headwater catchments in the southern Sierra Nevada,  
1035 *J. Am. Water Resour. Assoc.*, 52, 1327–1346, <https://doi.org/10.1111/1752-1688.12457>, 2016.

1036 Safeeq, M., Grant, G. E., Lewis, S. L., and Tague, C. L.: Coupling snowpack and groundwater dynamics to interpret historical  
1037 streamflow trends in the western United States: COUPLING SNOWPACK AND GROUNDWATER DYNAMICS TO  
1038 INTERPRET STREAMFLOW, *Hydrol. Process.*, 27, 655–668, <https://doi.org/10.1002/hyp.9628>, 2013.

1039 Santhi, C., Allen, P. M., Muttiah, R. S., Arnold, J. G., and Tuppap, P.: Regional estimation of base flow for the conterminous  
1040 United States by hydrologic landscape regions, *J. Hydrol. (Amst.)*, 351, 139–153,  
1041 <https://doi.org/10.1016/j.jhydrol.2007.12.018>, 2008.

1042 Sauquet, E., Shanafield, M., Hammond, J. C., Sefton, C., Leigh, C., and Detry, T.: Classification and trends in intermittent  
1043 river flow regimes in Australia, northwestern Europe and USA: A global perspective, *J. Hydrol. (Amst.)*, 597, 126170,  
1044 <https://doi.org/10.1016/j.jhydrol.2021.126170>, 2021.

1045 Seaber, P. R., Kapinos, F. P., and Knapp, G. L.: Hydrologic unit maps, US Geological Survey, <https://doi.org/10.3133/wsp2294>,  
1046 1987.

1047 Sebestyen, S. D., Shanley, J. B., Blume, T., Duncan, J. M., Jones, J., Segura, C., and Mast, M. A.: Introduction to the special  
1048 issue on research and observatory catchments, *Hydrol. Process.*, 39, <https://doi.org/10.1002/hyp.70069>, 2025.

1049 Shalev, G. and Kratzert, F.: Caravan MultiMet: Extending Caravan with multiple weather nowcasts and forecasts, arXiv  
1050 [cs.LG], arXiv, 2024.

1051 Shanley, J. B., Sebestyen, S. D., McDonnell, J. J., McGlynn, B. L., and Dunne, T.: Water’s Way at Sleepers River watershed  
1052 – revisiting flow generation in a post-glacial landscape, Vermont USA, *Hydrol. Process.*, 29, 3447–3459,  
1053 <https://doi.org/10.1002/hyp.10377>, 2015.

1054 Shapley, L. S.: 17. A Value for n-Person Games, in: *Contributions to the Theory of Games (AM-28)*, Volume II, edited by:  
1055 Kuhn, H. W. and Tucker, A. W., Princeton University Press, Princeton, 307–318, <https://doi.org/10.1515/9781400881970-018>,  
1056 1953.

1057 Shaw, S. B. and Riha, S. J.: Examining individual recession events instead of a data cloud: Using a modified interpretation of  
1058  $dQ/dt-Q$  streamflow recession in glaciated watersheds to better inform models of low flow, *J. Hydrol. (Amst.)*, 434-435, 46–  
1059 54, <https://doi.org/10.1016/j.jhydrol.2012.02.034>, 2012.

1060 Shrestha, D., Howard, D., and Benedict, T. D.: Moderate Resolution Imaging Spectroradiometer (MODIS) irrigated  
1061 Agriculture datasets for the conterminous United States (MirAD-US), <https://doi.org/10.5066/P9NA3EO8>, 2019.

1062 Sivapalan, M.: Pattern, process and function: Elements of a unified theory of hydrology at the catchment scale, in:  
1063 *Encyclopedia of Hydrological Sciences*, Wiley, Chichester, UK, <https://doi.org/10.1002/0470848944.hsa012>, 2005.

1064 Web Soil Survey: <http://websoilsurvey.nrcs.usda.gov/>, last access: 11 May 2025.

1065 Spieler, D., Mai, J., Craig, J. R., Tolson, B. A., and Schütze, N.: Automatic model structure identification for conceptual  
1066 hydrologic models, *Water Resour. Res.*, 56, <https://doi.org/10.1029/2019wr027009>, 2020.

1067 Stein, L., Clark, M. P., Knoben, W. J., Pianosi, F., & Woods, R. A.: How do climate and catchment attributes influence flood  
1068 generating processes? A large-sample study for 671 catchments across the contiguous USA. *Water Resources Research*, 57(4),  
1069 e2020WR028300. <https://doi.org/10.1029/2020WR028300>, 2021.

1070 Stets, E. G., Archer, A. A., Degnan, J. R., Erickson, M. L., Gorski, G., Medalie, L., and Scholl, M. A.: The National integrated  
1071 water availability assessment, 2025.

1072 Tague, C. and Grant, G. E.: A geological framework for interpreting the low-flow regimes of Cascade streams, Willamette  
1073 River Basin, Oregon: GEOLOGICAL FRAMEWORK FOR LOW-FLOW REGIMES, *Water Resour. Res.*, 40,  
1074 <https://doi.org/10.1029/2003wr002629>, 2004.

1075 Tague, C. and Grant, G. E.: Groundwater dynamics mediate low-flow response to climate warming in snow-dominated alpine  
1076 regions, *Water Resources Research*, 45, 2009.

1077 Tallaksen, L. M.: A review of baseflow recession analysis, *J. Hydrol.*, 165, 349–370, [https://doi.org/10.1016/0022-](https://doi.org/10.1016/0022-1694(94)02540-R)  
1078 [1694\(94\)02540-R](https://doi.org/10.1016/0022-1694(94)02540-R), 1995.

1079 Tarasova, L., Gnann, S., Yang, S., Hartmann, A., and Wagener, T.: Catchment characterization: Current descriptors,  
1080 knowledge gaps and future opportunities, *Earth Sci. Rev.*, 252, 104739, <https://doi.org/10.1016/j.earscirev.2024.104739>, 2023.

1081 Thompson, J. M., Hathaway, J. M., Perfect, E., and Schwartz, J. S.: The effect of stormwater infiltration and surrounding built  
1082 infrastructure on local groundwater dynamics: a case study for regenerative stormwater conveyances, *Sustain. Resilient*  
1083 *Infrastruct.*, 1–11, <https://doi.org/10.1080/23789689.2020.1772636>, 2020.

1084 Trancoso, R., Phinn, S., McVicar, T., Larsen, J., and McAlpine, C.: Regional variation in streamflow drivers across a  
1085 continental climatic gradient, *Ecohydrology*, 10, e1816, <https://doi.org/10.1002/eco.1816>, 2017.

1086 Tran, V. N.: CAMELSH: A large-sample hourly hydrometeorological dataset and attributes at watershed-scale for contiguous  
1087 United States, <https://doi.org/10.5281/ZENODO.15070091>, 2025.

1088 Tran, V. N., Xu, D., Van Nguyen, T., Kim, T., and Ivanov, V. Y.: CAMELSH: A large-sample hourly hydrometeorological  
1089 dataset and attributes at watershed-scale for CONUS, *Sci. Data*, 12, 1307, <https://doi.org/10.1038/s41597-025-05612-6>, 2025.

1090 Turner, S., Hannaford, J., Barker, L. J., Suman, G., Killeen, A., Armitage, R., Chan, W., Davies, H., Griffin, A., Kumar, A.,  
1091 Dixon, H., Albuquerque, M. T. D., Almeida Ribeiro, N., Alvarez-Garreton, C., Amoussou, E., Arheimer, B., Asano, Y.,  
1092 Berezowski, T., Bodian, A., Boutaghane, H., Capell, R., Dakhaoui, H., Daňhelka, J., Do, H. X., Ekkawatpanit, C., El Khalki,  
1093 E. M., Fleig, A. K., Fonseca, R., Giraldo-Osorio, J. D., Goula, A. B. T., Hanel, M., Horton, S., Kan, C., Kingston, D. G., Laaha,  
1094 G., Laugesen, R., Lopes, W., Mager, S., Rachdane, M., Markonis, Y., Medeiro, L., Midgley, G., Murphy, C., O'Connor, P.,  
1095 Pedersen, A. I., Pham, H. T., Piniewski, M., Renard, B., Saidi, M. E., Schmockler-Fackel, P., Stahl, K., Thyer, M., Toucher,  
1096 M., Trambly, Y., Uusikivi, J., Venegas-Cordero, N., Visessri, S., Watson, A., Westra, S., and Whitfield, P. H.: ROBIN:  
1097 Reference observatory of basins for international hydrological climate change detection, *Sci. Data*, 12, 654,  
1098 <https://doi.org/10.1038/s41597-025-04907-y>, 2025.

1099 UKIH: UK Institute of Hydrology (Great Britain), Low Flow Studies Reports, Institute of Hydrology, 1980.

1100 United States Department of Agriculture, Soil Survey Staff, and Natural Resources Conservation: U.S. General Soil Map  
1101 (STATSGO): Web soil survey, 2008.

1102 United States Geological Survey: Protected Areas Database of the United States (PAD-US) 4,  
1103 <https://doi.org/10.5066/P96WBCHS>, 2024.

1104 U.S. Environmental Protection Agency: National Hydrography Dataset Plus (NHDPlus): USEPA; USGS; and Horizon  
1105 Systems Corporation, 2008.

1106 U.S. Geological Survey: USGS Water Data for the Nation: U.S. Geological Survey National Water Information System  
1107 Database, <https://doi.org/10.5066/F7P55KJN>, 2025.

1108 Valeron, B. and Meixner, T.: Overland flow generation in chaparral ecosystems: temporal and spatial variability, *Hydrol.*  
1109 *Process.*, 24, 65–75, <https://doi.org/10.1002/hyp.7455>, 2010.

1110 Van Metre, P. C., Qi, S., Deacon, J., Dieter, C., Driscoll, J. M., Fienen, M., Kenney, T., Lambert, P., Lesmes, D., Mason, C.  
1111 A., Mueller-Solger, A., Musgrove, M., Painter, J., Rosenberry, D., Sprague, L., Tesoriero, A. J., Windham-Myers, L., and  
1112 Wolock, D.: Prioritizing river basins for intensive monitoring and assessment by the US Geological Survey, *Environ. Monit.*  
1113 *Assess.*, 192, 458, <https://doi.org/10.1007/s10661-020-08403-1>, 2020.

1114 Westerberg, I. K., Wagener, T., Coxon, G., McMillan, H. K., Castellarin, A., Montanari, A., and Freer, J.: Uncertainty in  
1115 hydrological signatures for gauged and ungauged catchments, *Water Resources Research*, 52, 1847–1865,  
1116 <https://doi.org/10.1002/2015WR017635>, 2016.

1117 Wiczorek, M. E. and LaMotte, A. E.: Attributes for NHDPlus Catchments (Version 1.1) for the Conterminous United States:  
1118 Average Saturation Excess-Overland Flow, 2002: U.S. Geological Survey data release, 2010.

1119 Wiczorek, M. E., Hafen, K. C., and Staub, L. E.: Data-Driven Drought Prediction Project model inputs for Upper and Lower  
1120 Colorado portions of the national hydrologic Geo-spatial fabric version 1.1 and select U.S. geological Survey streamgage basins  
1121 (ver. 2.0, July 2025), <https://doi.org/10.5066/P98IG8LO>, 2023.

1122 Willard, J. D., Ciulla, F., Weierbach, H., Kumar, V., and Varadharajan, C.: Evaluating deep learning approaches for predictions  
1123 in unmonitored basins with continental-scale stream temperature models, *arXiv [cs.LG]*, arXiv, 2024.

1124 Williams, P. W. and Ford, D. C.: Global distribution of carbonate rocks, *Zeitschrift für Geomorphologie Suppl.*, 147, 1–2, 2006.

1125 Wilson, C. G., Papanicolaou, A. N. T., and Denn, K. D.: Partitioning fine sediment loads in a headwater system with intensive  
1126 agriculture, *J. Soils Sediments*, 12, 966–981, <https://doi.org/10.1007/s11368-012-0504-2>, 2012.

1127 Winter, T. C.: The Concept of Hydrologic Landscapes, *JAWRA Journal of the American Water Resources Association*, 37,  
1128 335–349, <https://doi.org/10.1111/j.1752-1688.2001.tb00973.x>, 2001.

1129 Wlostowski, A. N., Molotch, N., Anderson, S. P., Brantley, S. L., Chorover, J., Dralle, D., Kumar, P., Li, L., Lohse, K. A.,  
1130 Mallard, J. M., McIntosh, J. C., Murphy, S. F., Parrish, E., Safeeq, M., Seyfried, M., Shi, Y., and Harman, C.: Signatures of  
1131 Hydrologic Function Across the Critical Zone Observatory Network, *Water Resour. Res.*, 57, e2019WR026635,  
1132 <https://doi.org/10.1029/2019wr026635>, 2021.

1133 Wolock, D. M.: Hydrologic landscape regions of the United States, US Geological Service, 2003a.

1134 Wolock, D. M.: Infiltration-excess overland flow estimated by TOPMODEL for the conterminous United States (No. 2003-  
1135 310), US Geological Survey., 2003b.

1136 Wu, S., Zhao, J., Wang, H., and Sivapalan, M.: Regional patterns and physical controls of streamflow generation across the  
1137 conterminous United States, *Water Resour. Res.*, 57, e2020WR028086, <https://doi.org/10.1029/2020wr028086>, 2021.

1138 Xia, Y., Mitchell, K., Ek, M., Sheffield, J., Cosgrove, B., Wood, E., Luo, L., Alonge, C., Wei, H., Meng, J., Livneh, B.,  
1139 Lettenmaier, D., Koren, V., Duan, Q., Mo, K., Fan, Y., and Mocko, D.: Continental-scale water and energy flux analysis and  
1140 validation for the North American Land Data Assimilation System project phase 2 (NLDAS-2): 1. Intercomparison and  
1141 application of model products, *J. Geophys. Res. D: Atmos.*, 117, <https://doi.org/10.1029/2011JD016048>, 2012.

1142 Xie, J., Liu, X., Jasechko, S., Berghuijs, W. R., Wang, K., Liu, C., Reichstein, M., Jung, M., and Koirala, S.: Majority of global  
1143 river flow sustained by groundwater, *Nat. Geosci.*, 17, 770–777, <https://doi.org/10.1038/s41561-024-01483-5>, 2024.

1144 Yang, L., Jin, S., Danielson, P., Homer, C., Gass, L., Bender, S. M., Case, A., Costello, C., Dewitz, J., Fry, J., Funk, M.,  
1145 Granneman, B., Liknes, G. C., Rigge, M., and Xian, G.: A new generation of the United States National Land Cover Database:  
1146 Requirements, research priorities, design, and implementation strategies, *ISPRS J. Photogramm. Remote Sens.*, 146, 108–123,  
1147 <https://doi.org/10.1016/j.isprsjprs.2018.09.006>, 2018.

1148 Yilmaz, K. K., Gupta, H. V., and Wagener, T.: A process-based diagnostic approach to model evaluation: Application to the  
1149 NWS distributed hydrologic model, *Water Resour. Res.*, 44, <https://doi.org/10.1029/2007wr006716>, 2008.

1150 Zimmer, M. A. and Gannon, J. P.: Run-off processes from mountains to foothills: The role of soil stratigraphy and structure  
1151 in influencing run-off characteristics across high to low relief landscapes, *Hydrol. Process.*, 32, 1546–1560,  
1152 <https://doi.org/10.1002/hyp.11488>, 2018.

1153 Zipper, S. C., Hammond, J. C., Shanafield, M., Zimmer, M., Datry, T., Jones, C. N., Kaiser, K. E., Godsey, S. E., Burrows, R.  
1154 M., Blaszcak, J. R., Busch, M. H., Price, A. N., Boersma, K. S., Ward, A. S., Costigan, K., Allen, G. H., Krabbenhoft, C. A.,  
1155 Dodds, W. K., Mims, M. C., Olden, J. D., Kampf, S. K., Burgin, A. J., and Allen, D. C.: Pervasive changes in stream  
1156 intermittency across the United States, *Environ. Res. Lett.*, 16, 084033, <https://doi.org/10.1088/1748-9326/ac14ec>, 2021.